

Minimum Error Entropy Rauch-Tung-Striebel Smoother

Jiacheng He, Hongwei Wang, Gang Wang, Shan Zhong, Bei Peng

Abstract—Outliers and impulsive disturbances often cause heavy-tailed distributions in practical applications, and these will degrade the performance of Gaussian approximation smoothing algorithms. To improve the robustness of the Rauch-Tung-Striebel (RTS) smoother against complicated non-Gaussian noises, a new RTS-smoother integrated with the minimum error entropy (MEE) criterion (MEE-RTS) is proposed for linear systems, which is also extended to the state estimation of nonlinear systems by utilizing the Taylor series linearization approach. The mean error behavior, the mean square error behavior, as well as the computational complexity of the MEE-RTS smoother are analyzed. According to simulation results, the proposed smoothers perform better than several robust solutions in terms of steady-state error.

Index Terms—Article submission, IEEE, IEEEtran, journal, LATEX, paper, template, typesetting.

I. INTRODUCTION

SMOOTHING algorithms are important techniques for estimating the state of dynamic systems, which have been applied in various industrial applications such as target tracking [1], system identification [2], positioning [3], and many others [4]–[6]. The Rauch-Tung-Striebel (RTS) smoother [7] is important for estimating the state of linear estimation with Gaussian noise. For nonlinear systems, some classic Gaussian smoothers are developed such as the extended RTS (ERTS) [8], the unscented RTS (URTS) [9], the cubature Kalman [10] smoothers and some iterative strategy-based smoothers [11].

These aforementioned smoothers perform well with the presence of both the Gaussian process and measurement noises. However, a class of non-Gaussian measurement noise with heavy-tailed distributions is common in practical applications [12]–[15]. Non-Gaussian noise will dramatically decrease the performance of the smoothers that are initially devised for Gaussian noises. To address this issue, some strategies have been developed. Robust statistics, especially M-estimations [16], [17], is one of the popular strategies to

develop robust smoother for non-Gaussian noises. Another popular approach is to use the heavy-tailed distributions to model the non-Gaussian process and measurement noises, such as the Laplace [18] distribution, Student's t distribution [19]–[21], and generalized Gaussian scale mixture distribution [22]. In addition, the robust smoothers based on H_∞ [23] and Gaussian mixture model have also been studied. In recent, the maximum correntropy criterion (MCC) [24], in information theoretic learning (ITL) [25], receives a great deal of attention, and some RTS-type smoothers are developed for nonlinear systems, such as maximum correntropy RTS (MC-RTS) [26] smoother, maximum mixture correntropy nonlinear smoother (MMC-ORNS) [27], and robust cubature Kalman smoother (RCKS) [12].

Although the MCC criterion is a good option for suppressing the effects of the heavy-tailed non-Gaussian noises [28], [29], it may not perform as well for more complicated noise [27], for example noises with multimodal distribution. In ITL, the minimum error entropy (MEE) criterion [30], [31], as an important cost function, has been applied in adaptive filtering [32]–[35], Kalman filter (KF) [36]–[38], and others [39], [40].

In addition, unscented KF [41] and cubature KF [42] are also combined with the MEE criterion to enhance the estimation performance of the nonlinear systems with non-Gaussian noise. However, the MEE-based smoother has not been investigated. Moreover, compared with the KF-type algorithms, the smoothers based on the RTS framework has an additional step called backward pass, and this additional step gives the smoother an improved performance than the corresponding KF-type algorithms. Hence, a novel RTS smoother using the MEE criterion as a cost function is investigated, which is expected to obtain superior performance.

In this study, a RTS-type smoother based the MEE criterion (MEE-RTS smoother) is proposed for the state estimation of the linear systems. Furthermore, an extended RTS smoother based on the MEE criterion is also developed for the nonlinear systems. Several theoretical analyses of the MEE-RTS smoother are presented, such as the mean error behavior, mean square error behavior, and computational complexity. Numerical simulations indicate the proposed smoothers outperform several existing robust smoothers in the mean-square deviation (MSD).

The remaining parts of this article are structured as follows. In Section II, the problem formulation on the proposed smoothers are given. Two new smoothers on the basis of the MEE criterion are presented in Section III. A few theoretical analysis of the MEE-RTS smoother are presented in Section IV. Simulations, conclusions, and acknowledgments are pre-

This work was funded by the NNSFC with Nos. 51975107 and 62103083, Sichuan Science and Technology Major Project No.2019ZDZX0020, and Sichuan Science and Technology Program, No. 2022YFG0343. The first two authors contributed equally to this study. (Corresponding author: Bei Peng.)

J. He, S. Zhong, and B. Peng are with School of Mechanical and Electrical Engineering, University of Electronic Science and Technology of China, Chengdu, 611731, PR China (e-mail: hejiacheng_123@163.com; 2608589754@qq.com; beipeng@uestc.edu.cn).

H. Wang is with National Key Laboratory of Science and Technology on Communications, University of Electronic Science and Technology of China, Chengdu, 611731, PR China (e-mail: tianhangxinxiang@163.com).

G. Wang is with School of Information and Communication Engineering, University of Electronic Science and Technology of China, Chengdu, 611731, PR China (e-mail: wanggang_hld@uestc.edu.cn).

Manuscript received April 19, 2021; revised August 16, 2021.

sented in Section V, Section VI, and Section VII.

II. PROBLEM FORMULATION

A discrete-time linear systems, in this paper, is consider, and it is described using the following state-space model

$$\begin{cases} \mathbf{x}_t = \mathbf{F}_t \mathbf{x}_{t-1} + \mathbf{q}_t, \\ \mathbf{y}_t = \mathbf{H}_t \mathbf{x}_t + \mathbf{r}_t, \end{cases} \quad (1)$$

where $\mathbf{x}_t \in \mathbb{R}^{n \times 1}$ represents the state of the linear systems at time t ; $\mathbf{y}_t \in \mathbb{R}^{m \times 1}$ denotes the measurement of interest; \mathbf{F}_t and \mathbf{H}_t denote the state transition matrix and measurement matrix; \mathbf{q}_t and \mathbf{r}_t represent, respectively, the process and measurement noises. Nominally, both \mathbf{q}_t and \mathbf{r}_t follow zero-mean Gaussian distributions, and their covariance matrices are \mathbf{Q}_t and \mathbf{R}_t , respectively. However, due to the impulse disturbance, outliers, or other factors, the distributions of \mathbf{q}_t and \mathbf{r}_t are generally no longer Gaussian, and reveal the heavy-tail properties. Such non-Gaussian distributions will degrade the performance of the existing RTS smoothers since they are initially devised under the Gaussian assumptions. To deal with the performance degradation, in this work, a robust smoother is developed to estimate the states $\mathbf{x}_{1:T} \triangleq \{\mathbf{x}_1, \dots, \mathbf{x}_T\}$ utilizing the measurements $\mathbf{y}_{1:T} \triangleq \{\mathbf{y}_1, \dots, \mathbf{y}_T\}$ with the presence of the heavy-tailed non-Gaussian noise. Specifically, we integrate the MEE criterion into the conventional RTS smoother framework to dampen the negative effect of the non-Gaussian noises.

III. MEE BASED ROBUST SMOOTHER

A. Minimum error entropy criterion

The quadratic Renyi's entropy [43], also known as the error entropy, is the definition of

$$H_2(e) = -\log V_2(e), \quad (2)$$

where error $e \triangleq X - Y$ denotes the error made between two random variables X and Y , and the information potential $V_2(e)$ is given by

$$V_2(e) = \int p^2(e) de = \mathbb{E}[p(e)], \quad (3)$$

where $p(e)$ represent the probability density function (PDF) on e , and $\mathbb{E}[\cdot]$ is an expectation operator. The PDF $p(e)$ can be estimated via the Parzen window strategy employing the error samples:

$$\hat{p}(e) = \frac{1}{L} \sum_{i=1}^L G(e - e_i), \quad (4)$$

where $G(e) = (1/\sqrt{2\pi}\sigma) \exp(-e^2/2\sigma^2)$ is the Gaussian kernel function, and parameter σ is the kernel bandwidth of $G(\cdot)$, and $\{e_i\}_{i=1}^L$ denote L independent and identically distributed (i.i.d.) error samples. With the estimated PDF in (4), one can obtain an estimate of $V_2(e)$ via (3) as

$$\hat{V}_2(e) = \frac{1}{L} \sum_{i=1}^L \hat{p}(e) = \frac{1}{L^2} \sum_{i=1}^L \sum_{j=1}^L G(e_i - e_j), \quad (5)$$

and the detailed derivation process can be found in [25].

In ITL, minimizing the error entropy can be used as a criterion for optimization, i.e., the MEE criterion, which is given by

$$\min H_2(e) = \max \log V_2(e). \quad (6)$$

Due to the fact that $\max \log V_2(e)$ is equivalent to $\max V_2(e)$ and $V_2(e)$ can be estimated via (5) with samples, the MEE criterion can be further expressed as

$$\max V_2(e) \approx \max \frac{1}{L^2} \sum_{i=1}^L \sum_{j=1}^L G(e_i - e_j). \quad (7)$$

The MEE criterion has unique advantages for handling complicated non-Gaussian noise [43], which motivates us to develop a new smoother based on the MEE criterion.

B. The MEE based RTS smoother

1) *Forward filtering procedure:* The forward filtering process is the foundation of the backward smoothing process, and its output $\{\tilde{\mathbf{x}}_{t|t}, \mathbf{P}_{t|t}\}$ are the input of the backward smoothing process. In the linear-regression-based KF solution, the measurement equation and filter update be recast as a regression problem [17]. Denote \mathbf{x}_t the real state of the system, and hence the state prediction error can be expressed as $\delta_t = \tilde{\mathbf{x}}_{t|t-1} - \mathbf{x}_t$, where $\tilde{\mathbf{x}}_{t|t-1}$ is the predicted state. With \mathbf{y}_t and $\tilde{\mathbf{x}}_{t|t-1}$, the regression problem with the form of

$$\begin{bmatrix} \mathbf{y}_t \\ \tilde{\mathbf{x}}_{t|t-1} \end{bmatrix} = \begin{bmatrix} \mathbf{H}_t \mathbf{x}_t \\ \mathbf{x}_t \end{bmatrix} + \begin{bmatrix} \mathbf{r}_t \\ \delta_t \end{bmatrix}. \quad (8)$$

Defining

$$\mathbf{M}_t = \begin{bmatrix} \mathbf{R}_t^{-\frac{1}{2}} & \mathbf{0} \\ \mathbf{0} & \mathbf{P}_{t|t-1}^{-\frac{1}{2}} \end{bmatrix}, \quad (9)$$

and multiplying \mathbf{M}_t on both sides of (8) will transform the linear regression problem in (8) as

$$\mathbf{d}_t = \mathbf{Z}_t \mathbf{x}_t + \mathbf{e}_t, \quad (10)$$

where

$$\mathbf{d}_t = \begin{bmatrix} \mathbf{R}_t^{-\frac{1}{2}} \mathbf{y}_t \\ \mathbf{P}_{t|t-1}^{-\frac{1}{2}} \tilde{\mathbf{x}}_{t|t-1} \end{bmatrix}, \quad (11)$$

$$\mathbf{Z}_t = \begin{bmatrix} \mathbf{R}_t^{-\frac{1}{2}} \mathbf{H}_t \\ \mathbf{P}_{t|t-1}^{-\frac{1}{2}} \end{bmatrix}, \quad (12)$$

and

$$\mathbf{e}_t = \begin{bmatrix} \mathbf{R}_t^{-\frac{1}{2}} & \mathbf{0}_n \\ \mathbf{0}_n & \mathbf{P}_{t|t-1}^{-\frac{1}{2}} \end{bmatrix} \begin{bmatrix} \mathbf{r}_t \\ \delta_t \end{bmatrix}. \quad (13)$$

From (10), the augmented error can be written as

$$\mathbf{e}_t = \mathbf{d}_t - \mathbf{Z}_t \mathbf{x}_t, \quad (14)$$

and hence the optimal estimation of $\tilde{\mathbf{x}}_{t|t}$ can be gained by the MEE criterion, which is formulated as

$$\begin{aligned}\tilde{\mathbf{x}}_{t|t} &= \arg \max_{\mathbf{x}_t} J_{MEE}(\mathbf{x}_t) \\ &= \arg \max_{\mathbf{x}_t} \frac{1}{N^2} \sum_{i=1}^N \sum_{j=1}^N G(e_{t;i} - e_{t;j}).\end{aligned}\quad (15)$$

where $e_{t;i} = d_{t;i} - \mathbf{z}_{t;i}\mathbf{x}_t$, $e_{t;i}$ and $d_{t;i}$ are the i th element of \mathbf{e}_t and \mathbf{d}_t , $\mathbf{z}_{t;i}$ represents the i th row of \mathbf{Z}_t . The variable N is equal to $m + n$.

Set the gradient of the cost function in (15) on \mathbf{e}_t will lead to

$$\frac{2}{N^2\sigma^2} \mathbf{Z}_t^T \Psi_t \mathbf{e}_t - \frac{2}{N^2\sigma^2} \mathbf{Z}_t^T \Phi_t \mathbf{e}_t = 0, \quad (16)$$

where the (i, j) th element of Ψ_t and Φ_t are, respectively, given by $[\Phi_t]_{ij} = G(e_{t;i} - e_{t;j})$ and

$$[\Psi_t]_{ij} = \begin{cases} \sum_{j=1}^N G(e_{t;i} - e_{t;j}), \\ 0, i \neq j, \end{cases}$$

Substitute (14) into (16) and one can reach at

$$\mathbf{x}_t = [\mathbf{Z}_t^T \Omega_t \mathbf{Z}_t]^{-1} \mathbf{Z}_t^T \Omega_t \mathbf{d}_t, \quad (17)$$

where Ω_t is expressed as

$$\begin{aligned}\Omega_t &= \Psi_t^T \Psi_t + \Phi_t^T \Phi_t \\ &= \begin{bmatrix} \Omega_{t;yy} & \Omega_{t;xy} \\ \Omega_{t;yx} & \Omega_{t;xx} \end{bmatrix}.\end{aligned}\quad (18)$$

Define $[\mathbf{Z}_t^T \Omega_t \mathbf{Z}_t]^{-1} \mathbf{Z}_t^T \Omega_t \mathbf{d}_t = l(\mathbf{x}_t)$, and thus Eq. (17) becomes a function on \mathbf{x}_t , so the estimated $\tilde{\mathbf{x}}_{t|t}$ can be obtained via the fixed-point iteration (FPI) method

$$(\tilde{\mathbf{x}}_{t|t})_{k+1} = l[(\tilde{\mathbf{x}}_{t|t})_k] = [\mathbf{Z}_t^T (\hat{\Omega}_t)_k \mathbf{Z}_t]^{-1} \mathbf{Z}_t^T (\hat{\Omega}_t)_k \mathbf{d}_t, \quad (19)$$

where variables with superscript \wedge denote variables that are affected by the introduction of the FPI method, e.g. $\hat{\Omega}_t$, where the subscript k is the number of the FPI method.

Combining (11), (12), and (18) yields

$$\begin{cases} \mathbf{Z}_t^T (\hat{\Omega}_t)_k \mathbf{Z}_t = \mathbf{H}_t^T (\hat{\mathbf{P}}_{t|t-1}^{yy})_k \mathbf{H}_t + (\hat{\mathbf{P}}_{t|t-1}^{yx})_k \mathbf{H}_t \\ + \mathbf{H}_t^T (\hat{\mathbf{P}}_{t|t-1}^{xy})_k + (\hat{\mathbf{P}}_{t|t-1}^{xx})_k, \\ \mathbf{Z}_t^T (\hat{\Omega}_t)_k \mathbf{d}_t = [\mathbf{H}_t^T (\hat{\mathbf{P}}_{t|t-1}^{yy})_k + (\hat{\mathbf{P}}_{t|t-1}^{yx})_k] \mathbf{y}_t \\ + [\mathbf{H}_t^T (\hat{\mathbf{P}}_{t|t-1}^{xy})_k + (\hat{\mathbf{P}}_{t|t-1}^{xx})_k] \tilde{\mathbf{x}}_{t|t-1}. \end{cases} \quad (20)$$

with

$$\begin{cases} (\hat{\mathbf{P}}_{t|t-1}^{xx})_k = [\mathbf{P}_{t|t-1}^{-\frac{1}{2}}]^T (\hat{\Omega}_{t;x})_k \mathbf{P}_{t|t-1}^{-\frac{1}{2}}, \\ (\hat{\mathbf{P}}_{t|t-1}^{xy})_k = [\mathbf{R}_t^{-\frac{1}{2}}]^T (\hat{\Omega}_{t;xy})_k \mathbf{P}_{t|t-1}^{-\frac{1}{2}}, \\ (\hat{\mathbf{P}}_{t|t-1}^{yx})_k = [\mathbf{P}_{t|t-1}^{-\frac{1}{2}}]^T (\hat{\Omega}_{t;yx})_k \mathbf{R}_t^{-\frac{1}{2}}, \\ (\hat{\mathbf{P}}_{t|t-1}^{yy})_k = [\mathbf{R}_t^{-\frac{1}{2}}]^T (\hat{\Omega}_{t;y})_k \mathbf{R}_t^{-\frac{1}{2}}. \end{cases} \quad (21)$$

Substituting (20) into (17) yields the update of $(\tilde{\mathbf{x}}_{t|t})_{k+1}$ as

$$(\tilde{\mathbf{x}}_{t|t})_{k+1} = \tilde{\mathbf{x}}_{t|t-1} + (\hat{\mathbf{K}}_t)_k (\mathbf{y}_t - \mathbf{H}_t \tilde{\mathbf{x}}_{t|t-1}), \quad (22)$$

where the Kalman gain is

$$(\hat{\mathbf{K}}_t)_k = [\mathbf{Z}_t^T (\hat{\Omega}_t)_k \mathbf{Z}_t]^{-1} [(\hat{\mathbf{P}}_{t|t-1}^{yx})_k + \mathbf{H}_t^T (\hat{\mathbf{P}}_{t|t-1}^{yy})_k]. \quad (23)$$

When the condition $\|(\tilde{\mathbf{x}}_{t|t})_{k+1} - (\tilde{\mathbf{x}}_{t|t})_k\| / \|(\tilde{\mathbf{x}}_{t|t})_k\| \leq \tau$ is satisfied, the FPI algorithm stops, and $\hat{\mathbf{K}}_t = (\hat{\mathbf{K}}_t)_k$. The covariance matrix $\mathbf{P}_{t|t}$ can be updated in the following way

$$\mathbf{P}_{t|t} = (\mathbf{I} - \hat{\mathbf{K}}_t \mathbf{H}_t) \mathbf{P}_{t|t-1} (\mathbf{I} - \hat{\mathbf{K}}_t \mathbf{H}_t)^T + \hat{\mathbf{K}}_t \mathbf{R}_t \hat{\mathbf{K}}_t^T. \quad (24)$$

2) *Backward smoothing procedure:* The backward smoothing procedure is performed after the forward filtering procedure. The objective of the backward smoothing procedure is the smoothing state $\tilde{\mathbf{x}}_{t|T}$ ($t = T-1, T-2, \dots, 1$) and covariance matrices $\mathbf{P}_{t|T}$ ($t = T-1, T-2, \dots, 1$).

Similar to the forward pass, the backward smoothing problem can be reformulated as a linear regression problem based on the smoothing state $\tilde{\mathbf{x}}_{t+1|T}$ and the filtering state $\tilde{\mathbf{x}}_{t|t}$. The regression problem takes the form

$$\begin{bmatrix} \tilde{\mathbf{x}}_{t+1|T} \\ \tilde{\mathbf{x}}_{t|t} \end{bmatrix} = \begin{bmatrix} \mathbf{F}_t \mathbf{x}_t \\ \mathbf{x}_t \end{bmatrix} + \begin{bmatrix} \boldsymbol{\rho}_t \\ \boldsymbol{\gamma}_t \end{bmatrix}, \quad (25)$$

where $\boldsymbol{\gamma}_t = \tilde{\mathbf{x}}_{t|t} - \mathbf{x}_t$ denotes the estimation error of $\tilde{\mathbf{x}}_{t|t}$, and $\boldsymbol{\rho}_t = \tilde{\mathbf{x}}_{t+1|T} - \mathbf{F}_t \mathbf{x}_t$ represents the prediction error of the state.

Define

$$\mathbf{Y}_t = \begin{bmatrix} \mathbf{Q}_t^{-\frac{1}{2}} & \mathbf{0} \\ \mathbf{0} & \mathbf{P}_{t|t}^{-\frac{1}{2}} \end{bmatrix}. \quad (26)$$

Both sides of (25) are simultaneously multiplied together by \mathbf{Y}_t , and we can get

$$\boldsymbol{\Theta}_t = \mathbf{W}_t \mathbf{x}_t + \boldsymbol{\varepsilon}_t \quad (27)$$

with

$$\boldsymbol{\Theta}_t = \begin{bmatrix} \mathbf{Q}_t^{-\frac{1}{2}} \tilde{\mathbf{x}}_{t+1|T} \\ \mathbf{P}_{t|t}^{-\frac{1}{2}} \tilde{\mathbf{x}}_{t|t} \end{bmatrix}, \quad (28)$$

$$\mathbf{W}_t = \begin{bmatrix} \mathbf{Q}_t^{-\frac{1}{2}} \mathbf{F}_t \\ \mathbf{P}_{t|t}^{-\frac{1}{2}} \end{bmatrix}, \quad (29)$$

and

$$\boldsymbol{\varepsilon}_t = \begin{bmatrix} \mathbf{Q}_t^{-\frac{1}{2}} & \mathbf{0} \\ \mathbf{0} & \mathbf{P}_{t|t}^{-\frac{1}{2}} \end{bmatrix} \begin{bmatrix} \boldsymbol{\rho}_t \\ \boldsymbol{\gamma}_t \end{bmatrix}. \quad (30)$$

From (27), the augmented error can be written as

$$\boldsymbol{\varepsilon}_t = \boldsymbol{\Theta}_t - \mathbf{W}_t \mathbf{x}_t. \quad (31)$$

Based on the MEE criterion, the optimal estimation of \mathbf{x}_t is obtained via

$$\begin{aligned}\tilde{\mathbf{x}}_{t|T} &= \arg \max_{\mathbf{x}_t} J_{MEE}(\mathbf{x}_t) \\ &= \arg \max_{\mathbf{x}_t} \frac{1}{L^2} \sum_{i=1}^L \sum_{j=1}^L G(\varepsilon_{t;i} - \varepsilon_{t;j}),\end{aligned}\quad (32)$$

where $\varepsilon_{t;i} = \theta_{t;i} - \mathbf{w}_{t;i}^T \mathbf{x}_t$, $\varepsilon_{t;i}$ and $\theta_{t;i}$ are the i th element of $\boldsymbol{\varepsilon}_t$ and $\boldsymbol{\Theta}_t$, $\mathbf{w}_{t;i}$ represents the i th row of \mathbf{W}_t , and $L = 2n$ is the dimension of $\boldsymbol{\varepsilon}_t$. The gradient of the cost function in (32) can be expressed as:

$$\begin{aligned}\frac{\partial J_{MEE}(\mathbf{x}_t)}{\partial \mathbf{x}_t} &= \frac{2}{L^2 \sigma^2} \sum_{i=1}^L \sum_{j=1}^L [\mathbf{w}_{t;j}^T G(\varepsilon_{t;j} - \varepsilon_{t;i}) \varepsilon_{t;j}] \\ &\quad - \frac{2}{L^2 \sigma^2} \sum_{i=1}^L \sum_{j=1}^L [\mathbf{w}_{t;j}^T G(\varepsilon_{t;j} - \varepsilon_{t;i}) \varepsilon_{t;i}].\end{aligned}\quad (33)$$

To further simplify, Eq. (33) can be further written as

$$\frac{\partial J_{MEE}(\mathbf{x}_t)}{\partial \mathbf{x}_t} = \frac{2}{L^2 \sigma^2} \mathbf{W}_t^T \boldsymbol{\Gamma}_t \boldsymbol{\varepsilon}_t - \frac{2}{L^2 \sigma^2} \mathbf{W}_t^T \boldsymbol{\Lambda}_t \boldsymbol{\varepsilon}_t \quad (34)$$

with

$$[\boldsymbol{\Gamma}_t]_{ij} = \begin{cases} \sum_{j=1}^L G(\varepsilon_{t;i} - \varepsilon_{t;j}), & i = j, \\ 0, & i \neq j, \end{cases} \quad (35)$$

and

$$[\boldsymbol{\Lambda}_t]_{ij} = G(\varepsilon_{t;i} - \varepsilon_{t;j}), \quad (36)$$

where $[\boldsymbol{\Gamma}_t]_{ij}$ and $[\boldsymbol{\Lambda}_t]_{ij}$ are the elements of the matrices $\boldsymbol{\Gamma}_t$ and $\boldsymbol{\Lambda}_t$, respectively.

To calculate $\tilde{\mathbf{x}}_{t|T}$ using (32), Eq. (34) is set to zero, and a numerically stable solution [44] can be obtained

$$\begin{cases} \boldsymbol{\Gamma}_t \boldsymbol{\varepsilon}_t = \boldsymbol{\Gamma}_t [\boldsymbol{\Theta}_t - \mathbf{W}_t \mathbf{x}_t] = 0, \\ \boldsymbol{\Lambda}_t \boldsymbol{\varepsilon}_t = \boldsymbol{\Lambda}_t [\boldsymbol{\Theta}_t - \mathbf{W}_t \mathbf{x}_t] = 0. \end{cases} \quad (37)$$

It is obvious that (37) can be further written as

$$\begin{bmatrix} \boldsymbol{\Gamma}_t \\ \boldsymbol{\Lambda}_t \end{bmatrix} \boldsymbol{\Theta}_t = \begin{bmatrix} \boldsymbol{\Gamma}_t \\ \boldsymbol{\Lambda}_t \end{bmatrix} \mathbf{W}_t \mathbf{x}_t. \quad (38)$$

Multiply both sides of (38) using $\mathbf{W}_t^T [\boldsymbol{\Gamma}_t^T \quad \boldsymbol{\Lambda}_t^T]$, and we can get

$$\mathbf{W}_t^T (\boldsymbol{\Gamma}_t^T \boldsymbol{\Gamma}_t + \boldsymbol{\Lambda}_t^T \boldsymbol{\Lambda}_t) \boldsymbol{\Theta}_t = \mathbf{W}_t^T (\boldsymbol{\Gamma}_t^T \boldsymbol{\Gamma}_t + \boldsymbol{\Lambda}_t^T \boldsymbol{\Lambda}_t) \mathbf{W}_t \mathbf{x}_t. \quad (39)$$

Further, the state of the system \mathbf{x}_t can be obtained by

$$\mathbf{x}_t = (\mathbf{W}_t^T \boldsymbol{\Xi}_t \mathbf{W}_t)^{-1} \mathbf{W}_t^T \boldsymbol{\Xi}_t \boldsymbol{\Theta}_t \quad (40)$$

with

$$\boldsymbol{\Xi}_t = \boldsymbol{\Gamma}_t^T \boldsymbol{\Gamma}_t + \boldsymbol{\Lambda}_t^T \boldsymbol{\Lambda}_t. \quad (41)$$

Since $(\mathbf{W}_t^T \boldsymbol{\Xi}_t \mathbf{W}_t)^{-1} \mathbf{W}_t^T \boldsymbol{\Xi}_t \boldsymbol{\Theta}_t$ is a function of \mathbf{x}_t , Eq. (40) can be further written as

$$\mathbf{x}_t = \mathbf{g}(\mathbf{x}_t) = (\mathbf{W}_t^T \boldsymbol{\Xi}_t \mathbf{W}_t)^{-1} \mathbf{W}_t^T \boldsymbol{\Xi}_t \boldsymbol{\Theta}_t. \quad (42)$$

To obtain the numerical solution of \mathbf{x}_t , two common methods are often used. One solution in [26], [45] is to use an approximate replacement method (ARM) that replaces \mathbf{x}_t contained in $\varepsilon_{t;i}$ by $\tilde{\mathbf{x}}_{t|t}$. The other solution is to use the FPI method to calculate the smoothing estimation $\tilde{\mathbf{x}}_{t|T}$, and one can obtain

$$(\tilde{\mathbf{x}}_{t|T})_k = [\mathbf{W}_t^T (\hat{\boldsymbol{\varepsilon}}_t)_k \mathbf{W}_t]^{-1} \mathbf{W}_t^T (\hat{\boldsymbol{\varepsilon}}_t)_k \boldsymbol{\Theta}_t, \quad (43)$$

where k denotes the number of the FPI method, and the initial value of the FPI is $(\tilde{\mathbf{x}}_{t|T})_{k=0} = \tilde{\mathbf{x}}_{t|t}$. When only one FPI loop is performed, the FPI turns into the ARM in [26], which indicates that the ARM is a special case of the FPI method.

Whether FPI or ARM is used, \mathbf{x}_t in (14) will be replaced by $\tilde{\mathbf{x}}_{t|t}$. The superscript \wedge is used to indicate the variable that has changed as a result of this substitution such as $\hat{\varepsilon}_{t;i}$, $\hat{\boldsymbol{\varepsilon}}_t$ etc.

To simplify the following derivation, $(\hat{\boldsymbol{\varepsilon}}_t)_k$ is written in the form of a block matrix as follows

$$(\hat{\boldsymbol{\varepsilon}}_t)_k = \begin{bmatrix} (\hat{\boldsymbol{\varepsilon}}_{t;x_1})_k & (\hat{\boldsymbol{\varepsilon}}_{t;x_1 x_2})_k \\ (\hat{\boldsymbol{\varepsilon}}_{t;x_2 x_1})_k & (\hat{\boldsymbol{\varepsilon}}_{t;x_2})_k \end{bmatrix}, \quad (44)$$

where $\hat{\boldsymbol{\varepsilon}}_{t;x_1} \in \mathbb{R}^{n \times n}$, $\hat{\boldsymbol{\varepsilon}}_{t;x_1 x_2} \in \mathbb{R}^{n \times n}$, $\hat{\boldsymbol{\varepsilon}}_{t;x_2 x_1} \in \mathbb{R}^{n \times n}$, and $\hat{\boldsymbol{\varepsilon}}_{t;x_2} \in \mathbb{R}^{n \times n}$.

Substitute (29) and (44) into $\mathbf{W}_t^T (\hat{\boldsymbol{\varepsilon}}_t)_k \mathbf{W}_t$ yields

$$\begin{aligned}\mathbf{W}_t^T (\hat{\boldsymbol{\varepsilon}}_t)_k \boldsymbol{\Theta}_t &= [\mathbf{F}_t^T (\hat{\mathbf{P}}_{t|t-1}^{b;x_1})_k + (\hat{\mathbf{P}}_{t|t-1}^{b;x_2 x_1})_k] \\ &\quad \times \tilde{\mathbf{x}}_{t+1|T} + [\mathbf{F}_t^T (\hat{\mathbf{P}}_{t|t-1}^{b;x_1 x_2})_k + (\hat{\mathbf{P}}_{t|t-1}^{b;x_2})_k] \tilde{\mathbf{x}}_{t|t}.\end{aligned} \quad (45)$$

with

$$\begin{cases} (\hat{\mathbf{P}}_{t|t-1}^{b;x_1})_k = (\mathbf{Q}_t^{-\frac{1}{2}})^T (\hat{\boldsymbol{\varepsilon}}_{t;x_1})_k \mathbf{Q}_t^{-\frac{1}{2}}, \\ (\hat{\mathbf{P}}_{t|t-1}^{b;x_2})_k = (\mathbf{P}_t^{-\frac{1}{2}})^T (\hat{\boldsymbol{\varepsilon}}_{t;x_2})_k \mathbf{P}_t^{-\frac{1}{2}}, \\ (\hat{\mathbf{P}}_{t|t-1}^{b;x_1 x_2})_k = (\mathbf{Q}_t^{-\frac{1}{2}})^T (\hat{\boldsymbol{\varepsilon}}_{t;x_1 x_2})_k \mathbf{P}_t^{-\frac{1}{2}}, \\ (\hat{\mathbf{P}}_{t|t-1}^{b;x_2 x_1})_k = (\mathbf{P}_t^{-\frac{1}{2}})^T (\hat{\boldsymbol{\varepsilon}}_{t;x_2 x_1})_k \mathbf{Q}_t^{-\frac{1}{2}}. \end{cases} \quad (46)$$

Similar to the process of obtaining (45), Eq. (47) can be obtained by substituting (28), (29), and (44) into $\mathbf{W}_t^T (\hat{\boldsymbol{\varepsilon}}_t)_k \boldsymbol{\Theta}_t$

$$\begin{aligned}\mathbf{W}_t^T (\hat{\boldsymbol{\varepsilon}}_t)_k \boldsymbol{\Theta}_t &= [\mathbf{F}_t^T (\hat{\mathbf{P}}_{t|t-1}^{b;x_1})_k + (\hat{\mathbf{P}}_{t|t-1}^{b;x_2 x_1})_k] \\ &\quad \times \tilde{\mathbf{x}}_{t+1|T} + [\mathbf{F}_t^T (\hat{\mathbf{P}}_{t|t-1}^{b;x_1 x_2})_k + (\hat{\mathbf{P}}_{t|t-1}^{b;x_2})_k] \tilde{\mathbf{x}}_{t|t}.\end{aligned} \quad (47)$$

The matrix inversion lemma [46] is utilized, and the following definitions

$$\begin{cases} \mathbf{A}_k = [(\hat{\mathbf{P}}_{t|t-1}^{b;x_2})_k + \mathbf{F}_t^T (\hat{\mathbf{P}}_{t|t-1}^{b;x_1 x_2})_k], \\ \mathbf{B}_k = [\mathbf{F}_t^T (\hat{\mathbf{P}}_{t|t-1}^{b;x_1})_k + (\hat{\mathbf{P}}_{t|t-1}^{b;x_2 x_1})_k], \\ \mathbf{C} = \mathbf{I}, \\ \mathbf{D} = \mathbf{F}_t. \end{cases} \quad (48)$$

$\left[\mathbf{W}_t^T(\hat{\mathbf{\Xi}}_t)_k \mathbf{W}_t\right]^{-1}$ can be further written as

$$\left[\mathbf{W}_t^T(\hat{\mathbf{\Xi}}_t)_k \mathbf{W}_t\right]^{-1} = \left(\mathbf{L}_t^b\right)_k = \mathbf{A}_k^{-1} - \left(\hat{\mathbf{K}}_t^b\right)_k \mathbf{F}_t \mathbf{A}_k^{-1} \quad (49)$$

with

$$\left(\hat{\mathbf{K}}_t^b\right)_k = \mathbf{A}_k^{-1} \mathbf{B}_k \left(\mathbf{I} + \mathbf{F}_t \mathbf{A}_k^{-1} \mathbf{B}_k\right)^{-1}, \quad (50)$$

where $\left(\hat{\mathbf{K}}_t^b\right)_k$ is defined as the smoothing gain.

From (50), one can obtain $\left(\hat{\mathbf{K}}_t^b\right)_k \left(\mathbf{I} + \mathbf{F}_t \mathbf{A}_k^{-1} \mathbf{B}_k\right) = \mathbf{A}_k^{-1} \mathbf{B}_k$. Multiply \mathbf{B}_k on both sides of (49), and we can obtain

$$\begin{aligned} \left(\mathbf{L}_t^b\right)_k \mathbf{B}_k &= \mathbf{A}_k^{-1} \mathbf{B}_k - \left(\hat{\mathbf{K}}_t^b\right)_k \mathbf{F}_t \mathbf{A}_k^{-1} \mathbf{B}_k \\ &= \left(\hat{\mathbf{K}}_t^b\right)_k + \left(\hat{\mathbf{K}}_t^b\right)_k \mathbf{F}_t \mathbf{A}_k^{-1} \mathbf{B}_k - \left(\hat{\mathbf{K}}_t^b\right)_k \mathbf{F}_t \mathbf{A}_k^{-1} \mathbf{B}_k \quad (51) \\ &= \left(\hat{\mathbf{K}}_t^b\right)_k. \end{aligned}$$

Combining (49), (47), and (51) leads to the updated strategy of $\tilde{\mathbf{x}}_t$

$$\begin{aligned} \mathbf{x}_{t|T} &= \left[\mathbf{W}_t^T(\hat{\mathbf{\Xi}}_t)_k \mathbf{W}_t\right]^{-1} \mathbf{W}_t^T(\hat{\mathbf{\Xi}}_t)_k \boldsymbol{\Theta}_t \\ &= \left(\mathbf{L}_t^b\right)_k \mathbf{B}_k \tilde{\mathbf{x}}_{t+1|T} + \left(\mathbf{L}_t^b\right)_k \mathbf{A}_k \tilde{\mathbf{x}}_{t|t} \\ &= \left(\hat{\mathbf{K}}_t^b\right)_k \tilde{\mathbf{x}}_{t+1|T} + \left[\mathbf{A}_k^{-1} - \left(\hat{\mathbf{K}}_t^b\right)_k \mathbf{F}_t \mathbf{A}_k^{-1}\right] \mathbf{A}_k \tilde{\mathbf{x}}_{t|t} \\ &= \tilde{\mathbf{x}}_{t|t} + \left(\hat{\mathbf{K}}_t^b\right)_k \left(\tilde{\mathbf{x}}_{t+1|T} - \tilde{\mathbf{x}}_{t+1|t}\right). \end{aligned} \quad (52)$$

where $\left(\hat{\mathbf{K}}_t^b\right)_k$ is

$$\begin{aligned} \left(\hat{\mathbf{K}}_t^b\right)_k &= \left[\mathbf{W}_t^T(\hat{\mathbf{\Xi}}_t)_k \mathbf{W}_t\right]^{-1} \\ &\times \left[\mathbf{F}_t^T \left(\hat{\mathbf{P}}_{t|t-1}^{b;x_1}\right)_k + \left(\hat{\mathbf{P}}_{t|t-1}^{b;x_2;x_1}\right)_k\right]. \end{aligned} \quad (53)$$

When condition $\left\|\left(\tilde{\mathbf{x}}_{t|T}\right)_{k+1} - \left(\tilde{\mathbf{x}}_{t|T}\right)_k\right\| / \left\|\left(\tilde{\mathbf{x}}_{t|T}\right)_k\right\| \leq \tau$ is satisfied, the the FPI algorithm stops, and $\hat{\mathbf{K}}_t^b = \left(\hat{\mathbf{K}}_t^b\right)_k$.

The error covariance of smoothed estimate $\tilde{\mathbf{x}}_{t|T}$ can be obtained by

$$\mathbf{P}_{t|T} = \mathbf{P}_{t|t} + \mathbf{K}_t^b \left(\mathbf{P}_{t+1|N} - \mathbf{P}_{t+1|t}\right) \left(\mathbf{K}_t^b\right)^T. \quad (54)$$

The detailed derivation of (54) is shown in A.

According to the above derivation, the pseudo-code of the MEE-RTS smoother is summarized in Algorithm 1.

C. The MEE based extended RTS smoother

For state estimation of the nonlinear systems, the process and measurement equations can be described as

$$\begin{cases} \mathbf{x}_t = \mathbf{f}(\mathbf{x}_{t-1}) + \mathbf{q}_{t-1}, \\ \mathbf{y}_t = \mathbf{h}(\mathbf{x}_t) + \mathbf{r}_t. \end{cases} \quad (57)$$

where mapping $\mathbf{f}(\cdot)$ denotes a known nonlinear state transition function, mapping $\mathbf{h}(\cdot)$ is a known nonlinear measurement function. The ERTS is a frequently utilized tool for the state smoothing problems for the nonlinear systems. In the

Algorithm 1: RTS smoother based on the MEE

Input: state transition matrix \mathbf{F}_t , measurement matrix \mathbf{H}_t , covariance matrices \mathbf{Q}_t , \mathbf{R}_t , and kernel bandwidth σ

Output: $\tilde{\mathbf{x}}_{t|T}$

1 **Initialization:** $\tilde{\mathbf{x}}_{0|0} = \mathbf{x}_0$, $\mathbf{P}_{0|0} = \mathbf{P}_0$;

2 **Forward Pass:** for $t \leftarrow 1$ to T do

3 Calculate $\tilde{\mathbf{x}}_{t|t-1}$ and $\mathbf{P}_{t|t-1}$ using

$$\begin{cases} \tilde{\mathbf{x}}_{t|t-1} = \mathbf{F}_t \tilde{\mathbf{x}}_{t-1|t-1}, & (55a) \\ \mathbf{P}_{t|t-1} = \mathbf{F}_t \mathbf{P}_{t-1|t-1} \mathbf{F}_t^T + \mathbf{Q}_t; & (55b) \end{cases}$$

4 **while** $\left\|\left(\tilde{\mathbf{x}}_{t|t}\right)_{k+1} - \left(\tilde{\mathbf{x}}_{t|t}\right)_k\right\| / \left\|\left(\tilde{\mathbf{x}}_{t|t}\right)_k\right\| \geq \tau$ **do**

5 Update $\left(\tilde{\mathbf{x}}_{t|t}\right)_{k+1}$ using (14), (18), (21), (22), and (23);

6 **end**

7 Update $\mathbf{P}_{t|t}$ using (24);

8 **end**

9 **Backward Pass:** for $t \leftarrow T - 1$ to 1 do

10 Calculate $\tilde{\mathbf{x}}_{t+1|t}$ and $\mathbf{P}_{t+1|t}$ utilizing (55);

11 Let $k = 1$ and $\left(\tilde{\mathbf{x}}_{t|T}\right)_{k=0} = \tilde{\mathbf{x}}_{t|t}$;

12 **while** $\left\|\left(\tilde{\mathbf{x}}_{t|T}\right)_{k+1} - \left(\tilde{\mathbf{x}}_{t|T}\right)_k\right\| / \left\|\left(\tilde{\mathbf{x}}_{t|T}\right)_k\right\| \geq \tau$ **do**

13 Update $\left(\tilde{\mathbf{x}}_{t|T}\right)_{k+1}$ using (52) with (53), (44), (46), and (31);

14 **end**

15 Calculate $\mathbf{P}_{t|T}$ utilizing (54);

16 **end**

ERTS, the nonlinear functions $\mathbf{f}(\cdot)$ is linearized by the first-order Taylor series expansion at $\tilde{\mathbf{x}}_{t-1|t-1}$, i.e.,

$$\mathbf{f}(\mathbf{x}_{t-1}) \approx \mathbf{f}(\tilde{\mathbf{x}}_{t-1|t-1}) + \mathbf{F}_{t-1} (\mathbf{x}_{t-1} - \tilde{\mathbf{x}}_{t-1|t-1}), \quad (58)$$

where the Jacobian matrix of the nonlinear function $\mathbf{f}(\cdot)$ is obtained via

$$\mathbf{F}_{t-1} = \left. \frac{\partial \mathbf{f}(\mathbf{x}_{t-1})}{\partial \mathbf{x}} \right|_{\mathbf{x}=\tilde{\mathbf{x}}_{t-1|t-1}}. \quad (59)$$

Combining (57) and (58) yields:

$$\mathbf{x}_t \approx \mathbf{f}(\tilde{\mathbf{x}}_{t-1|t-1}) + \mathbf{F}_{t-1} (\mathbf{x}_{t-1} - \tilde{\mathbf{x}}_{t-1|t-1}) + \mathbf{q}_{t-1}. \quad (60)$$

Substitute (60) into (57) and the augmented model for the MEE-ERTS can be written as

$$\begin{aligned} \boldsymbol{\varepsilon}_t^l &= \begin{bmatrix} \mathbf{Q}_t^{-\frac{1}{2}} & \mathbf{0}_n \\ \mathbf{0}_n & \mathbf{P}_{t|t}^{-\frac{1}{2}} \end{bmatrix} \begin{bmatrix} \tilde{\mathbf{x}}_{t+1|T} - \mathbf{f}(\mathbf{x}_t) \\ \tilde{\mathbf{x}}_{t|t} - \mathbf{x}_t \end{bmatrix} \\ &= \begin{bmatrix} \mathbf{Q}_t^{-\frac{1}{2}} & \mathbf{0}_n \\ \mathbf{0}_n & \mathbf{P}_{t|t}^{-\frac{1}{2}} \end{bmatrix} \begin{bmatrix} \tilde{\mathbf{x}}_{t+1|T} - \mathbf{f}(\tilde{\mathbf{x}}_{t|t}) - \mathbf{F}_t (\mathbf{x}_t - \tilde{\mathbf{x}}_{t|t}) \\ \tilde{\mathbf{x}}_{t|t} - \mathbf{x}_t \end{bmatrix}. \end{aligned} \quad (61)$$

and we also obtain

$$\tilde{\boldsymbol{\varepsilon}}_t^l = \boldsymbol{\Theta}_t^l - \mathbf{W}_t^l (\tilde{\mathbf{x}}_{t|t})_k \quad (62)$$

Algorithm 2: Extended RTS smoother based on the MEE

Input: $f(\cdot)$, $h(\cdot)$, Q_t , R_t , and σ
Output: $\tilde{x}_{t|T}$

- 1 **Initialization:** $\tilde{x}_{0|0} = x_0$, $P_{0|0} = P_0$;
- 2 **Forward Pass:** for $t \leftarrow 1$ to T do
- 3 These steps of the MEE-EKF algorithm are presented in [43].
- 4 **end**
- 5 **Backward Pass:** for $t \leftarrow T - 1$ to 1 do
- 6 Predicting the state of the system using
 $\tilde{x}_{t+1|t} = f(\tilde{x}_{t|t})$;
- 7 Calculate the Jacobian matrix and covariance matrix using (59) and
 $P_{t|t-1} = F_{t-1} P_{t-1|t-1} F_{t-1}^T + Q$;
- 8 Let $k = 1$ and $(\tilde{x}_{t|T})_{k=0} = \tilde{x}_{t|t}$;
- 9 **while** $\|(\tilde{x}_{t|T})_{k+1} - (\tilde{x}_{t|T})_k\| / \|(\tilde{x}_{t|T})_k\| \geq \tau$ **do**
- 10 Update $(\tilde{x}_{t|T})_{k+1}$ using
 $(\tilde{x}_{t|T})_{k+1} = \tilde{x}_{t|t} + \hat{K}_t^b (\tilde{x}_{t+1|T} - \tilde{x}_{t+1|t})$ with
 $\begin{cases} \hat{K}_t^b = (W_t^T \hat{\Sigma}_t W_t)^{-1} (F_t^T \hat{P}_{t|t-1}^{b;x_1} + \hat{P}_{t|t-1}^{b;x_2 x_1}), \\ \hat{\Sigma}_t = \hat{\Gamma}_t^T \hat{\Gamma}_t + \hat{\Lambda}_t^T \hat{\Lambda}_t, [\hat{\Lambda}_t]_{ij} = G[\hat{\varepsilon}_{t,i}^l - \hat{\varepsilon}_{t,j}^l], \\ [\hat{\Gamma}_t]_{ij} = \begin{cases} \sum_{j=1}^L G_\sigma[\hat{\varepsilon}_{t,i}^l - \hat{\varepsilon}_{t,j}^l], i = j, \\ 0, i \neq j, \end{cases} \\ \hat{P}_{t|t-1}^{b;x_1} = (Q_t^{-\frac{1}{2}})^T \hat{\Sigma}_{t;x_1} Q_t^{-\frac{1}{2}}, \\ \hat{\varepsilon}_{t,i} = \theta_{t,i} - w_{t,i}(\tilde{x}_{t|T})_k, \\ \hat{P}_{t|t-1}^{b;x_2 x_1} = (P_{t|t}^{-\frac{1}{2}})^T \hat{\Sigma}_{t;x_2 x_1} Q_t^{-\frac{1}{2}}, \end{cases}$
- 11 **end**
- 12 Update covariance matrix using
 $P_{t|T} \approx P_{t|t} + \hat{K}_t^b (P_{t+1|N} - P_{t+1|t}) (\hat{K}_t^b)^T$ (56)
- 13 **end**

with

$$\Theta_t^l = \begin{bmatrix} Q_t^{-\frac{1}{2}} [\tilde{x}_{t+1|T} - f(\tilde{x}_{t|t}) + F_t \tilde{x}_{t|t}] \\ P_{t|t}^{-\frac{1}{2}} \tilde{x}_{t|t} \end{bmatrix} \quad (63)$$

and

$$W_t^l = \begin{bmatrix} Q_t^{-\frac{1}{2}} F_t \\ P_{t|t}^{-\frac{1}{2}} \end{bmatrix}. \quad (64)$$

It is apparent that (62) have a similar form as the one in (31). Hence, the derivation process of the backward pass of the MEE-ERTS smoother is similar to that of the backward pass of the MEE-RTS smoother. In order to avoid the repetition, the derivation process of the MEE-ERTS smoother is omitted and its pseudo-code is presented in Algorithm 2.

Remark 1: It is notable that the threshold τ , in both Algorithm 1 and Algorithm 2, is a vital parameter to control the number of the FPI method. The larger the threshold is, the fewer the number of FPI are required, and therefore the less computational burden of the algorithms, which in turn reduces the performance of the proposed smoothers in steady-state errors to some extent, whereas a smaller threshold means the opposite.

IV. THEORETICAL ANALYSIS

A. Mean error behavior

In this part, $\xi_{s;t} = x_t - \tilde{x}_{t|T}$ is employed to present the estimation error of smoother, and $\xi_{f;t} = x_t - \tilde{x}_{t|t}$ denotes the estimation error of filter. According to (51), $\xi_{s;t}$ can be rewritten as:

$$\begin{aligned} \xi_{s;t} &= x_t - \tilde{x}_{t|T} \\ &= \xi_{f;t} - \hat{K}_t^b (\tilde{x}_{t+1|T} - \tilde{x}_{t+1|t}). \end{aligned} \quad (65)$$

According to $\tilde{x}_{t|t-1} = F_t \tilde{x}_{t-1|t-1}$, $\xi_{f;t-1} = x_{t-1} - \tilde{x}_{t-1|t-1}$, and $x_t = F_t x_{t-1} + q_t$, one can obtain

$$\tilde{x}_{t+1|t} = x_{t+1} - q_{t+1} - F_t \xi_{f;t}. \quad (66)$$

Substituting (66) into (65) yields

$$\xi_{s;t} = (I - \hat{K}_t^b F_t) \xi_{f;t} + \hat{K}_t^b \xi_{s;t+1} - \hat{K}_t^b q_{t+1}. \quad (67)$$

Since the process and measurement noises are zero mean, the expectation of estimation error $\xi_{s;t}$ can be expressed as

$$E[\xi_{s;t}] = (I - \hat{K}_t^b F_t) E[\xi_{f;t}] + \hat{K}_t^b E[\xi_{s;t+1}]. \quad (68)$$

From (46), it is obvious that $\hat{P}_{t|t-1}^{b;x_1}$ and $\hat{P}_{t|t-1}^{b;x_2}$ are both strictly diagonally dominant. One can obtain

$$\hat{K}_t^b F_t \approx (F_t^T \hat{P}_{t|t-1}^{b;x_1} F_t + \hat{P}_{t|t-1}^{b;x_2})^{-1} (F_t^T \hat{P}_{t|t-1}^{b;x_1} F_t). \quad (69)$$

Substituting (69) into (68) yields

$$\begin{aligned} E[\xi_{s;t}] &\approx \left[I - (F_t^T \hat{P}_{t|t-1}^{b;x_1} F_t + \hat{P}_{t|t-1}^{b;x_2})^{-1} (F_t^T \hat{P}_{t|t-1}^{b;x_1} F_t) \right] \\ &\times E[\xi_{f;t}] + \left[(F_t^T \hat{P}_{t|t-1}^{b;x_1} F_t + \hat{P}_{t|t-1}^{b;x_2})^{-1} (F_t^T \hat{P}_{t|t-1}^{b;x_1} F_t) \right] \times \\ &F_t^{-1} E[\xi_{s;t+1}]. \end{aligned} \quad (70)$$

From (70), one can obtain that $E[\xi_{s;t}]$ is the linear combination of $E[\xi_{f;t}]$ and $E[\xi_{s;t+1}]$. Assuming that F_t is stable, one can conclude that both $F_t^T \hat{P}_{t|t-1}^{b;x_1} F_t$ and $\hat{P}_{t|t-1}^{b;x_2}$ are positive semi-definite, which will lead to the fact that (69) is stable. Further, (70) is also stable, which means that the proposed MEE-RTS smoother operates stably.

B. Mean square error behavior

According to (67), the error covariance matrix of the state can be written as

$$\begin{aligned} E[\xi_{s;t}\xi_{s;t}^T] = & \left(I - E[\hat{K}_t^b] F_t \right) E[\xi_{f;t}\xi_{f;t}^T] \left(I - E[\hat{K}_t^b] F_t \right)^T \\ & + E[\hat{K}_t^b] E[\xi_{s;t+1}\xi_{s;t+1}^T] E[\hat{K}_t^b]^T \\ & + E[\hat{K}_t^b] Q_t E[\hat{K}_t^b]^T. \end{aligned} \quad (71)$$

A convergent gain of smoother K_t^b can be obtained utilizing the fixed-point algorithm, and the expectation of gain $E[K_t^b]$ can be obtained by using the adaptive solution

$$E[K_t^b] = (1 - \iota) E[K_{t-1}^b] + \iota K_t^b, \quad (72)$$

where ι is the forgotten factor.

Formula (71) can be simplified as

$$N_t = \Omega_t N_{t-1} \Omega_t^T + Y_t \quad (73)$$

with

$$\begin{cases} N_t = E[\xi_{s;t}\xi_{s;t}^T], \\ \Omega_t = E[\hat{K}_t^b], \\ Y_t = \left(I - E[\hat{K}_t^b] F_t \right) E[\xi_{f;t}\xi_{f;t}^T] \left(I - E[\hat{K}_t^b] F_t \right)^T \\ \quad + E[\hat{K}_t^b] Q_t E[\hat{K}_t^b]^T. \end{cases} \quad (74)$$

From the matrix vector operator:

$$\begin{cases} \text{vec}(SUV) = (V^T \otimes S) \text{vec}(U), \\ \text{vec}(S + V) = \text{vec}(S) + \text{vec}(V), \end{cases} \quad (75)$$

where \otimes represents the Kronecker product and $\text{vec}(\cdot)$ denotes vectorization operation.

The closed-form solution of (73) can be written as

$$\lim_{t \rightarrow \infty} \text{vec}(N_t) = \lim_{t \rightarrow \infty} (I - \Omega_t \otimes \Omega_t)^{-1} \text{vec}(Y_t), \quad (76)$$

where $\text{vec}(Y_t)$ can be calculated by using (75), and one can obtain

$$\text{vec}(Y_t) = \xi_t \text{vec}[E[\xi_{f;t}\xi_{f;t}^T]] + \varsigma_t \text{vec}(Q_t) \quad (77)$$

with

$$\begin{cases} \xi_t = \left(I - E[\hat{K}_t^b] F_t \right) \otimes \left(I - E[\hat{K}_t^b] F_t \right), \\ \varsigma_t = E[\hat{K}_t^b] \otimes E[\hat{K}_t^b]. \end{cases} \quad (78)$$

The error covariance matrix $E[\xi_{f;t}\xi_{f;t}^T]$, in (77), has been calculated in [44].

C. Computational complexity

In this section, the computational burden of the proposed MEE-RTS smoother is compared with that of the RTS smoother and MC-RTS smoother for the linear systems. It is noted that the MC-RTS smoother in [26] is developed to estimate the state of the nonlinear systems, and the scheme for using MC-RTS smoother to handle state estimation of linear systems is not given. The pseudo-code for the MC-RTS smoother used to estimate the state of the linear systems (MC-RTSL) is summarised in Algorithm 3, which is used as the baseline in terms of computational burden and steady-state error. In Algorithm 3, $K_{t;MC}$ and $K_{t;MC}^b$ are gains of forward and backward pass.

From Algorithm 3, the computational burden of the forward pass and backward pass of the MC-RTSL smoother are

$$\begin{cases} S_{MC_F} = 8n^3 + 10n^2m + 6nm^2 + 2m^2 - n^2 \\ \quad + 4mn - n + m + 10 + 3O(n^3) + O(n^3), \\ S_{MC_B} = 12n^3 + 7n^2 + n + 10 + 4O(n^3), \end{cases} \quad (79)$$

where S_{MC_F} and S_{MC_B} represent the computational complexity of the forward pass and backward pass. Hence, the computational complexity of MC-RTSL smoother is

$$S_{MC-RTSL} = 20n^3 + 10n^2m + 6nm^2 + 2m^2 + 6n^2 + 4mn + m + 20 + 5O(n^3) + 3O(m^3). \quad (80)$$

The computational complexity of the forward pass of the MEE-RTS smoother is

$$\begin{aligned} S_{R-MEEKF} = & (7M_f + 8)n^3 + 7M_fm^3 - n^2 \\ & + (19M_f + 6)n^2m + (15M_f + 2)nm^2 \\ & + M_fO(n^3) + M_fm + (5M_f - 1)n \\ & + (7M_f - 1)nm + 3M_fO(m^3). \end{aligned} \quad (81)$$

where M_f is the number of the FPI method of the forward pass. The main formulas for the backward pass and their computational complexity are shown in Table I, and the computational burden of the backward pass of the MEE-RTS smoother is

$$\begin{aligned} S_{MEE_B} = & (48M_b + 8)n^3 + (1 - 6M_b)n^2 \\ & + (1 - 9M_b)n + 3M_bO(n^3) + 24M_b, \end{aligned} \quad (82)$$

where M_b denotes the number of the FPI method of the backward pass. Combining (81) and (82), the computational complexity of the MEE-RTS smoother is

$$\begin{aligned} S_{MEE-RTS} = & (7M_f + 48M_b + 16)n^3 + 7M_fm^3 \\ & + (19M_f + 6)n^2m - 6M_bn^2 + (15M_f + 2)nm^2 \\ & + (M_f + 3M_b)O(n^3) + M_fm + (5M_f - 9M_b)n \\ & + (7M_f - 1)nm + 3M_fO(m^3) + 24M_b. \end{aligned} \quad (83)$$

From (80) and (83), we can conclude that the computational complexity of the MEE-RTS smoother is slightly higher than that of MC-RTSL smoother. The main reasons for this phenomenon are the adoption of the MEE criterion and the FPI method of the R-MEEKF algorithm. In the MEE-RTS smoother, the MEE criterion is introduced into the forward and backward pass, and the MEE criterion with double summation is more computationally expensive than the MCC criterion

Algorithm 3: MC-RTS smoother for linear systems

Input: state transition matrix F , measurement matrix H , covariance matrices Q , R , and kernel bandwidth σ

Output: $\tilde{x}_{t|T}$

```

1 Initialization:  $\tilde{x}_{0|0} = x_0$ ,  $P_{0|0} = P_0$ ;
2 Forward Pass: for  $t \leftarrow 1$  to  $T$  do
3   Calculate  $\tilde{x}_{t|t-1}$  and  $P_{t|t-1}$  using (55);
4   Calculate  $K_{t;MC}$  and  $\phi_R$  using
      
$$\begin{cases} K_{t;MC} = (P_{t|t-1} + H^T \phi_R R^{-1} H)^{-1} H^T \phi_R R^{-1}, \\ \phi_R = G(\|y_t - Hx_{t|t-1}\|_R); \end{cases} \quad (84)$$

5
6   Calculate  $\tilde{x}_{t|t}$  and  $P_{t|t}$  using
      
$$\begin{cases} \tilde{x}_{t|t} = \tilde{x}_{t|t-1} + K_{t;MC} (y_t - H\tilde{x}_{t|t-1}), \\ P_{t|t} = K_{t;MC} R_t K_{t;MC}^T + \\ (I_n - K_{t;MC} H) P_{t|t-1} (I_n - K_{t;MC} H)^T; \end{cases} \quad (85)$$

7 end
8 Backward Pass: for  $t \leftarrow T - 1$  to 1 do
9   Calculate  $\phi_Q$  and  $K_{t;MC}^b$  using
      
$$\begin{cases} \phi_Q = G(\|\tilde{x}_{t+1|T} - F\tilde{x}_{t|t}\|_Q), \\ K_{t;MC}^b = (P_{t|t}^{-1} + F^T \phi_Q Q^{-1} F)^{-1} F^T \phi_Q Q^{-1}; \end{cases} \quad (86)$$

10
    Calculate  $\tilde{x}_{t|T}$  and  $P_{t|T}$  using
      
$$\begin{cases} \tilde{x}_{t|T} = \tilde{x}_{t|t} + K_{t;MC}^b (\tilde{x}_{t+1|T} - F\tilde{x}_{t|t}), \\ P_{t|T} = K_{t;MC}^b (P_{t+1|T} - P_{t+1|t}) (K_{t;MC}^b)^T \\ + P_{t|t}; \end{cases} \quad (87)$$

11 end

```

with a single summation. The increase in computational burden due to the introduction of the MEE is inevitable. In addition, the computational burden of the FPI method is higher than or equal to the computational complexity of ARM.

From the above discussion, one can be deduced that reducing the number of the FPI method (the number can be controlled by the parameter τ in [43]) or using ARM can significantly lower the computational complexity of the MEE-RTS algorithm. However, these two solutions also decrease the performance of the MEE-RTS smoother in steady-state error. Hence, the choice of parameter τ should therefore trade-off the steady-state error and the computational complexity of the MEE-RTS smoother, the detailed selection scheme of the parameter τ is present in Section V-D.

TABLE I
COMPUTATIONAL COMPLEXITIES OF THE MEE-RTS ALGORITHM.

	\times	$+$ and $-$	matrix inversion, Cholesky decomposition, and exponentiation
(55b)	n^2	$n^2 - n$	0
(55b)	$2n^3$	$2n^3 - n^2$	0
(52)	n^2	$n^2 + n$	0
(53)	$8n^3$	$8n^3 - 4n^2$	$3O(n^3)$
(41)	$16n^3$	$16n^3 - 4n^2$	0
(35)	$2n + 7$	$2n + 1$	4
(36)	$2n + 7$	$2n + 1$	4
(54)	$2n^3$	$2n^3$	0

V. SIMULATION

In this section, several numerical simulations are performed to demonstrate the performance of the proposed algorithms. In each run, 1000 samples are used to calculate the MSD of the MEE-RTS and MEE-ERTS smoothers. Simulation results are averaged over 300 independent Monte Carlo runs. The MSD [47] is defined as

$$MSD = 10 \log_{10} (\|x_t - \tilde{x}_{t|T}\|^2). \quad (88)$$

A. Noise model

A few non-Gaussian noise models are presented below before performing the simulation, such as mixed-Gaussian noise, α -stable noise and Rayleigh noise.

1 Modeling mixed-Gaussian noise [33] as follows:

$$r \sim \lambda \mathcal{N}(a_1, \mu_1) + (1 - \lambda) \mathcal{N}(a_2, \mu_2), 0 \leq \lambda \leq 1, \quad (89)$$

where parameter λ presents the mixing factor. The noise with a mixed-Gaussian distribution can be represented as $r \sim M(\lambda, a_1, a_2, \mu_1, \mu_2)$.

2 The characteristic function of the α -stable noise [48] is defined as:

$$\psi(t) = \exp \{ j\vartheta t - \gamma |t|^{\alpha_3} [1 + jb \operatorname{sgn}(t) S(t, a_3)] \}, \quad (90)$$

with

$$S(t, a_3) = \begin{cases} \tan(\frac{a_3 \pi}{2}), & a_3 \neq 1, \\ \frac{2}{\pi} \log |t|, & a_3 = 1, \end{cases} \quad (91)$$

where a_3 is the characteristic factor, b represents the symmetry parameter, γ and ϑ are the dispersion parameter and location parameter. The noise with α -stable distribution is expressed as $r \sim S(a_3, b, \gamma, \vartheta)$.

3 The Rayleigh distribution can be represented by the probability density function shown below:

$$r(t) = \frac{t}{\sigma^2} \exp\left(-\frac{t^2}{2\sigma^2}\right). \quad (92)$$

The noise with the Rayleigh distribution is written as $v \sim R(\sigma)$.

B. Example 1

In this sub-section, a constant acceleration motion model [37] is considered. The state-space model are given by

$$\mathbf{x}_t = \begin{bmatrix} 1 & \Delta T & \Delta T^2/2 \\ 0 & 1 & \Delta T \\ 0 & 0 & 1 \end{bmatrix} \mathbf{x}_{t-1} + \mathbf{q}_{t-1}, \quad (93)$$

and

$$\mathbf{y}_t = \begin{bmatrix} 1 & 0 & 0 \\ 0 & 1 & 0 \end{bmatrix} \mathbf{x}_t + \mathbf{r}_t. \quad (94)$$

Here, $\Delta T = 0.1 \text{ sec}$ represents sampling interval of the model, $\mathbf{x}_t = [x_{1;t} \ x_{2;t} \ x_{3;t}]^T$ with $x_{1;t}$, $x_{2;t}$, and $x_{3;t}$ denote position, velocity, and acceleration respectively.

Five scenarios with different noise models are considered. The specific forms of process and measurement noises are shown below:

$$\begin{cases} q_{t;i} \sim M(0.9, 0, 0, 0.01, 25), \\ r_{t;i} \sim \mathcal{N}(0, 0.01), \end{cases} \quad (95)$$

where $q_{t;i}$ and $r_{t;i}$ represent the i th element of \mathbf{q}_t and \mathbf{r}_t . The second scenario is that process and measurement noises are both mixed-Gaussian noise, which takes the following form

$$\begin{cases} q_{t;i} \sim M(0.9, 0, 0, 0.01, 25), \\ r_{t;i} \sim M(0.7, 0, 0, 0.01, 900). \end{cases} \quad (96)$$

The third scenario is that both the process noise is mixed-Gaussian noise, and the measurement noise is a mixture of α -stable noise and Gaussian noise with the following form

$$\begin{cases} q_{t;i} \sim M(0.9, 0, 0, 0.01, 25), \\ r_{t;i} \sim 0.9S(1.25, 1, 0, 0.5) + 0.1\mathcal{N}(0, 900). \end{cases} \quad (97)$$

where 0.9 denotes the probability that the noise $r_{t;i}$ obeys the distribution of $S(1.25, 1, 0, 0.5)$, and the representation below has a similar meaning. The fourth simulation scenario has the following form:

$$\begin{cases} q_{t;i} \sim M(0.9, 0, 0, 0.01, 25), \\ r_{t;i} \sim 0.7R(2) + 0.3\mathcal{N}(0, 900). \end{cases} \quad (98)$$

The fifth scenario is that the process noise obeys a mixed-Gaussian distribution and the measurement noise is a multi-modal distribution of the following form

$$\begin{cases} q_{t;i} \sim M(0.95, 0, 0, 0.01, 25), \\ r_{t;i} \sim M(0.6, 2, -2, 0.01, 100). \end{cases} \quad (99)$$

The initial state \mathbf{x}_0 , initial estimated value $\tilde{\mathbf{x}}_{0|0}$, and initial covariance $\mathbf{P}_{0|0}$ of the above mentioned five scenarios are given by:

$$\begin{cases} \mathbf{x}_0 \sim \mathcal{N}(0, \mathbf{I}_n), \\ \tilde{\mathbf{x}}_{0|0} \sim \mathcal{N}(\mathbf{x}_0, \mathbf{Q}), \\ \mathbf{P}_{0|0} = \mathbf{I}_n. \end{cases} \quad (100)$$

In these five scenarios, we compare the performance of the MEE-RTS smoother with that of the KF, RTS smoother [7], MCKF [37], MC-RTS smoother [26], R-MEEKF [44] algorithms. These results are shown in Fig. 1, Fig. 2, and Table II.

First, the performance of the MEE-RTS smoother in a heavy-tailed noise environment is studied, and the simulation results are shown in Fig. 1 and Fig. 2. The convergence curves of MSD of x_1 , x_2 , and x_3 are presented in Figs. 1a, 1b, and 1c. Fig. 1d shows the variation curve of the MSD of \mathbf{x} with the mixture coefficient λ of measurement noise r_t . Some parameters of the considered algorithms are also presented in Fig. 1. It is obvious that the proposed MEE-RTS smoother performs best in the second scenario. From Fig. 1, one can witness that the performance of these algorithms degrades as the number of outliers increases. For the third scenario, the corresponding results and the parameter settings of these considered algorithms are shown in Fig. 2, and the effect of the mixture coefficient λ of the observed noise r_i with respect to the performance of the MEE-RTS smoother was studied. Similar results to the second scenario can be obtained from Fig. 2.

Then the robustness of the MEE-RTS smoother in different scenarios is investigated, and the simulation results are presented in Table II. The elements in Table II represent the MSD of x_1 , x_2 , and x_3 for the different algorithms in the considered scenarios, for example $(-20.1, -20.1, -20.1)$ represents the MSD of x_1 , x_2 , and x_3 of the KF algorithm in the first scenario. In particular, 2.0 in 0.9(2.0) denotes the kernel width of the R-MEE and RTS algorithms in the fifth scenario. From Table II, we can get that 1): the MEE-RTS smoother performs best with the non-Gaussian noise; 2): in a Gaussian noise environment, the MEE-RTS algorithm performs nearly as well as the RTS algorithm. These two points show that the MEE-RTS smoother is robust in different scenarios.

C. Example 2

In this part, a vehicle tracking model [49] is considered to verify the performance of the MEE-ETRS smoother, and the dataset [50] of a vehicle is obtained from the the measurements of lidar and radar sensors. The state equation can be expressed as

$$\mathbf{x}_t = \begin{bmatrix} 1 & 0 & \Delta T & 0 \\ 0 & 1 & 0 & \Delta T \\ 0 & 0 & 1 & 0 \\ 0 & 0 & 0 & 1 \end{bmatrix} \mathbf{x}_{t-1} + \mathbf{q}_{t-1}, \quad (101)$$

and the measurement equation of a radar is

$$\mathbf{y}_{t;\text{radar}} = \begin{bmatrix} \sqrt{x_{1;t}^2 + x_{2;t}^2} \\ \arctan\left(\frac{x_{2;t}}{x_{1;t}}\right) \\ \frac{x_{1;t}x_{3;t} + x_{2;t}x_{4;t}}{\sqrt{x_{1;t}^2 + x_{2;t}^2}} \end{bmatrix} + \mathbf{r}_{t;\text{radar}}, \quad (102)$$

and of a lidar is given by

$$\mathbf{y}_{t;\text{lidar}} = \begin{bmatrix} 1 & 0 & 0 & 0 \\ 0 & 1 & 0 & 0 \end{bmatrix} \mathbf{x}_t + \mathbf{r}_{t;\text{lidar}}, \quad (103)$$

for lidar. $\mathbf{r}_{t;\text{radar}}$ and $\mathbf{r}_{t;\text{lidar}}$ are measurement noises of radar and lidar, and they obey distributions $\mathbf{r}_{t;\text{lidar}} \sim M(0.9 \ 0 \ 0.01\mathbf{I}_3 \ 9\mathbf{r}_{\text{radar}})$ and $\mathbf{r}_{t;\text{lidar}} \sim M(0.9 \ 0 \ 0.01\mathbf{I}_2 \ 9\mathbf{r}_{\text{lidar}})$. Here, the

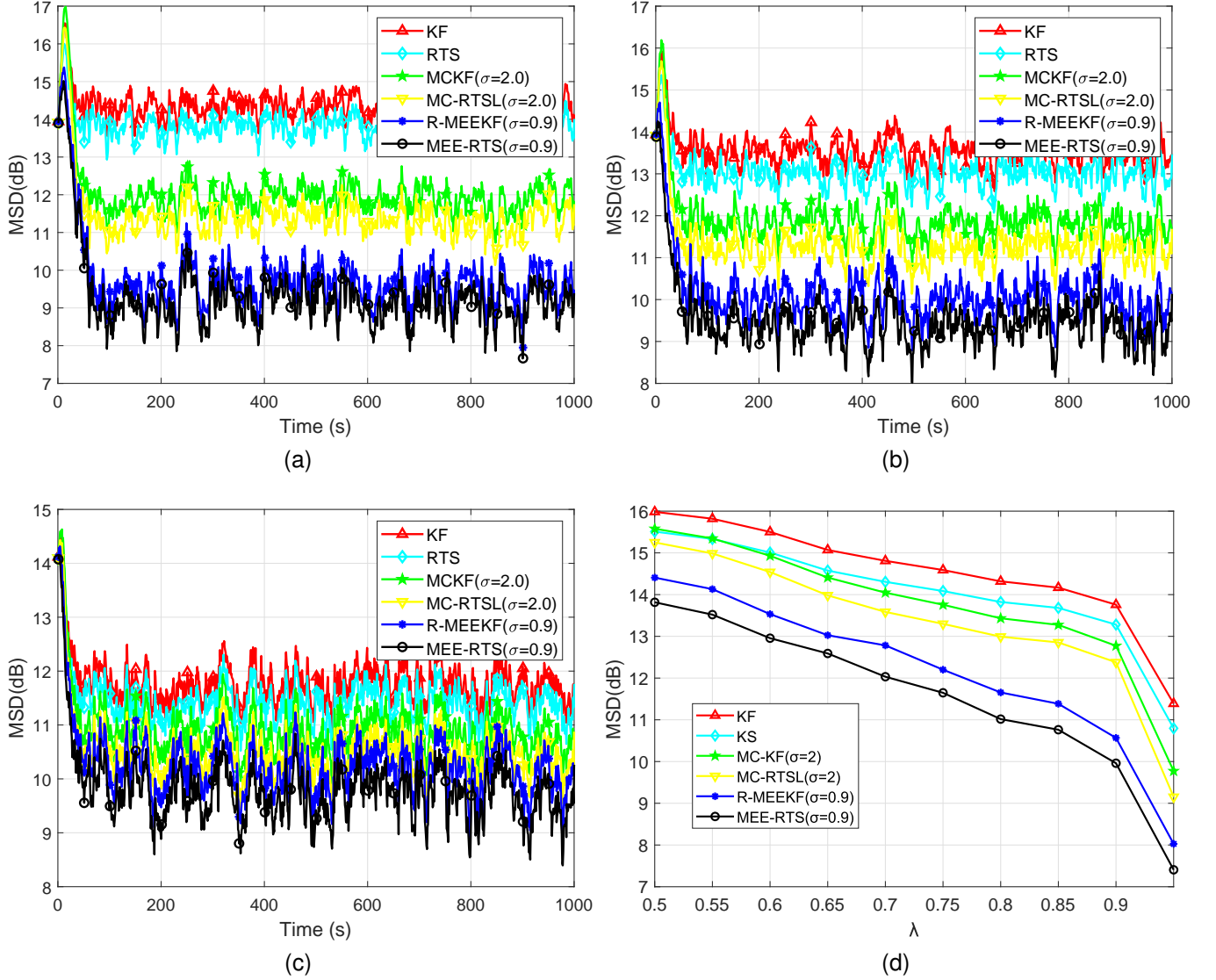


Fig. 1. MSD of different algorithms in second scenario. (a) MSD of x_1 . (b) MSD of x_2 . (c) MSD of x_3 . (d) The MSD with different λ .

matrices \mathbf{r}_{radar} and \mathbf{r}_{lidar} are $diag[1 \ 0.01 \ 0.01]$ and $diag[1 \ 0.01]$.

The state of vehicle can be represented as $\mathbf{x}_t = [x_{1,t}, x_{2,t}, x_{3,t}, x_{4,t}]^T$. $x_{1,t}$ and $x_{2,t}$ represent the position of x , y axis, $x_{3,t}$ and $x_{4,t}$ denote the velocity of x , y axis. The sampling interval is $\Delta T = 0.1$ sec, the covariance matrix of process noise is

$$\mathbf{Q} = \begin{bmatrix} \frac{\Delta T^2}{4} & 0 & \frac{\Delta T^3}{2} & 0 \\ 0 & \frac{\Delta T^2}{4} & 0 & \frac{\Delta T^3}{2} \\ \frac{\Delta T^3}{2} & 0 & \Delta T^2 & 0 \\ 0 & \frac{\Delta T^3}{2} & 0 & \Delta T^2 \end{bmatrix}.$$

The initial values of \mathbf{x}_0 , $\tilde{\mathbf{x}}_{0|0}$, and $\mathbf{P}_{0|0}$ are the same as (100). The covariance matrix of measurement noise is set to $\mathbf{R}_t = [0.09, 0.05, 0.09]$.

The variation curves of the MSD of different algorithms are presented in Fig. 3. According to Fig. 3, one can obtain that the MEE-RTS smoother outperforms several algorithms in terms of steady-state error.

D. Parameter selection

In this part, the influence of the critical parameters σ and τ on the performance of the MEE-RTS smoother is investigated, and guidance is given on the choice of parameters.

The influence of the kernel bandwidth σ on the performance of the MEE-RTS smoother is investigated in the above five scenarios, and the simulation results are displayed in Table III and Fig. 4a. As seen in Table III, one can be inferred that the performance of the MEE-RTS smoother first increases and then decreases in the increase of the parameter σ with the presence of non-Gaussian noise. The MEE-RTS smoother can yield the required performance when σ is close to 0.9 or 2.0. In a Gaussian noise environment, the performance of the MEE-RTS smoother improves with the increasing σ but does not exceed that of the RTS smoother and KF algorithms. The relationship between algorithm performance and kernel bandwidth guides the selection of kernel bandwidth. The selection scheme about σ is as follows: 1) a larger σ should

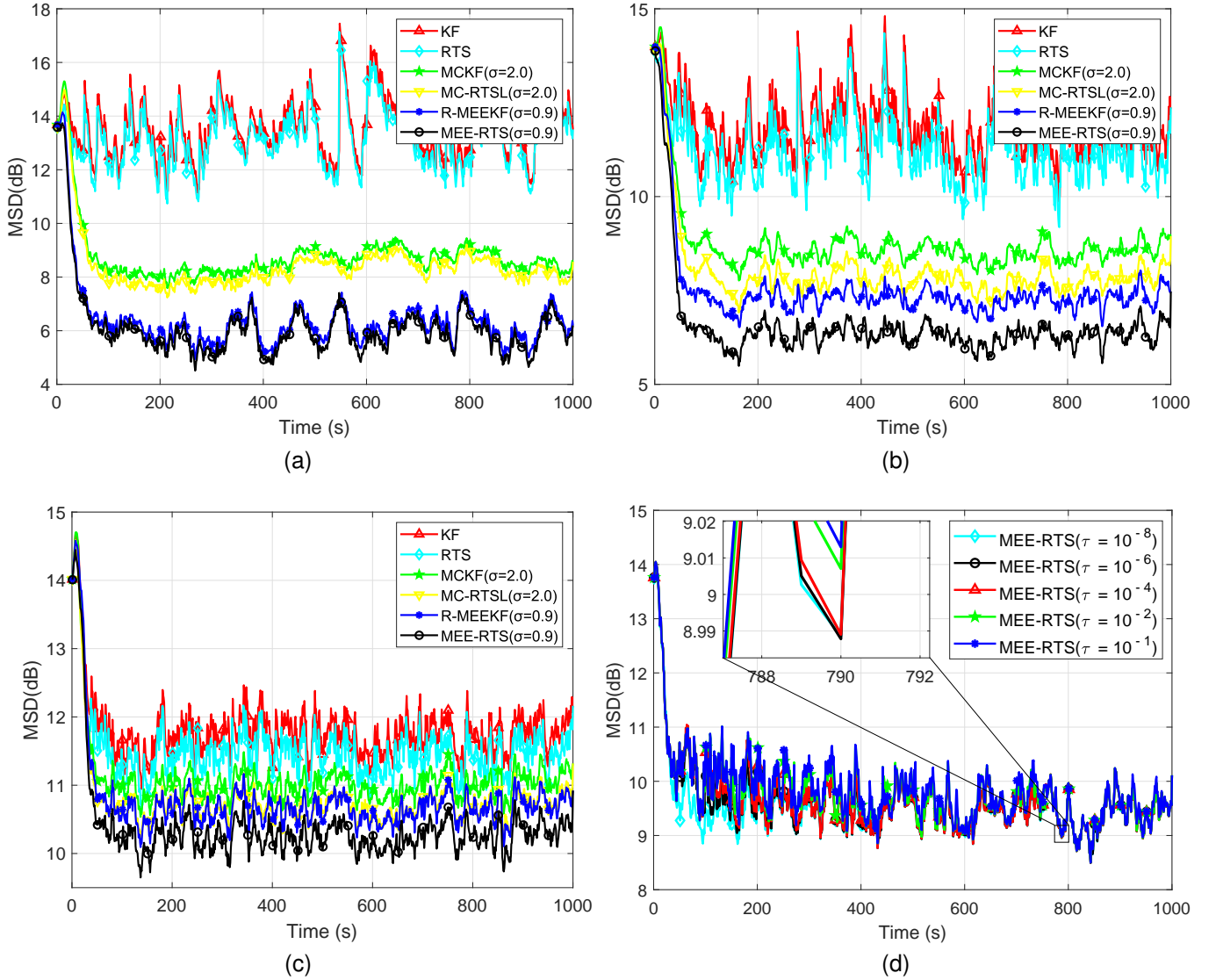


Fig. 2. The MSD of these considered algorithms in third scenario. (a) MSD of x_1 . (b) MSD of x_2 . (c) MSD of x_3 . (d) The MSD with different λ .

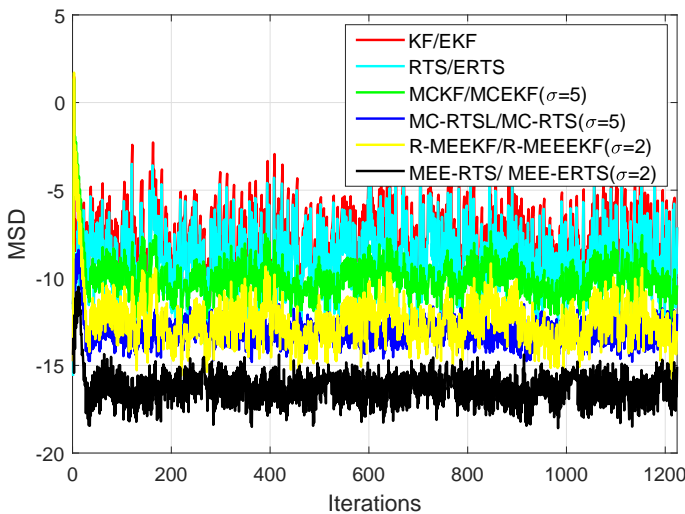


Fig. 3. MSD of different algorithms.

be set in a Gaussian noise environment; 2) the optimal kernel width is different in different heavy-tailed noise scenarios, and suitable σ is 0.9 or 2.0 in the considered scenarios.

The influence of threshold τ with respect to the performance of the MEE-RTS algorithm is also investigated in the presence of non-Gaussian noise. The simulation results are presented in Fig. 4b and Table IV with different τ . In the second scenario, Fig. 4b presents the MSD of MEE-RTS smoother with different τ and $\sigma = 0.9$. The MSD, computational time, and the number M of the FPI method of RTS, MC-RTSL, and MEE-RTS smoothers are presented in Table IV. These smoothers are measured using MATLAB 2020a, which works on an i5-8400 and a 2.80GHz CPU. From Fig. 4 and Table IV, the performance of the MEE-RTS smoother in steady-state MSD decreases to some extent as the threshold decreases in non-Gaussian noise environments, however, the cost (the computational complexity and computational time) of such a small increase in performance is expensive. Hence, the choice of threshold should trade off the steady-state MSD

TABLE II
THE STEADY-STATE MSD (DB) OF DIFFERENT ALGORITHMS IN DIFFERENT SCENARIOS

Algorithm	σ	First scenario	Second scenario	Third scenario	Fourth scenario	Fifth scenario
KF	N/A	(-20.1,-20.1,-20.1)	(11.5,14.8,12.0)	(15.8,13.3,9.0)	(13.3,14.8,14.4)	(9.0,8.6,8.2)
RTS	N/A	(-20.1,-20.2,-20.2)	(14.4,11.4,10.9)	(15.3,12.9,8.8)	(14.3,13.8,12.9)	(8.3,7.9,7.6)
MCKF	2.0	(-19.2,-19.2,-19.2)	(14.0,11.2,10.9)	(12.5,11.7,8.6)	(14.0,13.7,12.9)	(8.8,8.6,7.9)
MC-RTS	2.0	(-19.3,-19.3,-19.3)	(13.5,10.3,10.1)	(12.0,11.2,8.5)	(13.4,13.1,12.4)	(8.1,7.8,7.3)
R-MEEKF	0.9(2.0)	(-19.0,-19.0,-19.0)	(10.5,10.2,10.5)	(9.0,9.4,8.8)	(12.2,12.6,12.2)	(8.5,8.5,7.7)
MEE-RTS	0.9(2.0)	(-19.2,-19.1,-19.0)	(9.5,9.3,9.7)	(8.4,8.5,7.9)	(10.8,11.0,11.5)	(7.9,7.7,7.1)

TABLE III
THE STEADY-STATE MSD (DB) OF DIFFERENT ALGORITHMS WITH DIFFERENT KERNEL BANDWIDTH

Algorithm	σ	First scenario	Second scenario	Third scenario	Fourth scenario	Fifth scenario
RTS	N/A	(-20.1,-20.2,-20.2)	(14.4,11.4,10.9)	(15.3,12.9,8.8)	(14.3,13.1,12.4)	(8.3,7.9,7.6)
MC-RTS	2	(-19.3,-19.3,-19.3)	(13.5,10.3,10.1)	(12.0,11.2,8.5)	(13.4,13.1,12.4)	(8.1,7.8,7.3)
MEE-RTS	0.1	(-19.2,-19.1,-19.0)	(17.1,14.6,13.3)	(18.3,17.3,15.4)	(18.3,17.2,15.5)	(13.7,13.2,12.1)
MEE-RTS	0.5	(-19.2,-19.1,-19.0)	(13.1,11.4,11.3)	(11.7,11.9,12.3)	(11.9,11.7,12.1)	(13.1,11.9,11.2)
MEE-RTS	0.9	(-19.2,-19.1,-19.0)	(9.5,9.3,9.7)	(8.4,8.5,7.9)	(10.8,11.0,11.5)	(11.5,10.4,10.2)
MEE-RTS	2.0	(-19.3,-19.3,-19.1)	(13.3,9.5,9.2)	(11.9,12.0,11.8)	(12.0,11.9,11.7)	(7.9,7.7,7.1)
MEE-RTS	5.0	(-19.4,-19.4,-19.3)	(14.6,9.4,10.0)	(13.9,13.6,12.8)	(14.0,13.5,12.8)	(8.9,8.7,8.5)
MEE-RTS	50.0	(-19.5,-19.6,-19.7)	(17.9,11.9,11.3)	(14.6,14.3,13.3)	(14.7,14.3,13.4)	(9.1,9.1,8.8)
MEE-RTS	100.0	(-19.9,-19.9,-19.8)	(18.3,13.5,12.1)	(15.2,15.1,15.1)	(16.5,15.1,14.7)	(9.2,9.5,9.8)

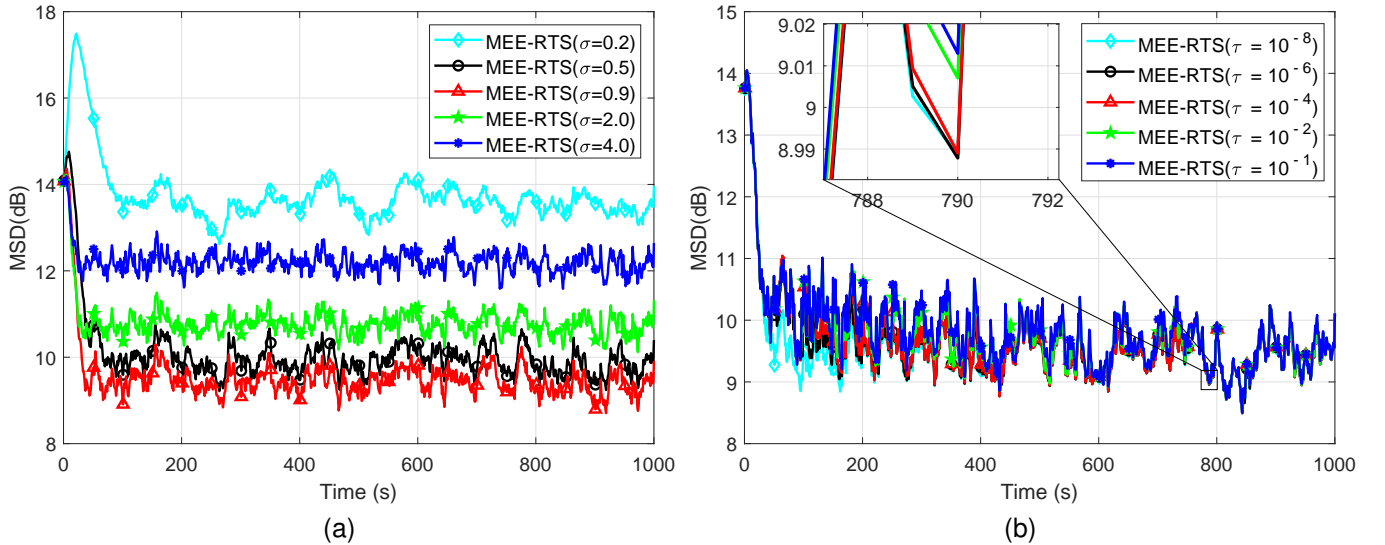


Fig. 4. MSD of MEE-RTS smoother with different σ . (a) MSD of MEE-RTS smoother with different σ . (b) MSD of the MEE-RTS smoother with different τ .

and cost, with smaller thresholds being chosen to improve the performance of the algorithm where real-time requirements are low, and larger thresholds or ARM being used in the opposite direction.

VI. CONCLUSION

In this study, two new RTS-type smoothers based on the MEE criterion were developed for estimating the state of the linear and nonlinear systems with non-Gaussian noise. Some theoretical analysis of the MEE-RTS smoother were given, and the results of these analyses have indicated that the MEE-RTS smoother is stable. Numerical simulation results have

indicated that the proposed smoothers perform better than several existing smoothers with non-Gaussian noise.

The choice of threshold τ should trade off the steady-state MSD and computational complexity of the MEE-RTS smoother, with smaller threshold being chosen to improve the performance of the algorithm where real-time requirements are low, and larger thresholds or ARM being used in the opposite direction. Furthermore, the kernel width σ has a significant influence on the steady-state MSD. Kernel width that are either too large or too small can degrade the performance of the MEE-RTS smoother and should be adjusted empirically.

The MEE-ERTS smoother is also developed for nonlinear

TABLE IV
THE STEADY-STATE MSD, COMPUTATIONAL TIME, AND THE NUMBER OF THE FPI METHOD OF DIFFERENT ALGORITHMS WITH DIFFERENT τ

	τ	Second scenario			Third scenario			Fourth scenario		
Algorithm		MSD	time (sec)	M	MSD	time (sec)	M	MSD	time (sec)	M
RTS	N/A	13.29	1.685×10^{-5}	N/A	12.94	1.643×10^{-5}	N/A	13.52	1.691×10^{-5}	N/A
MC-RTSL	N/A	11.07	7.499×10^{-5}	N/A	10.89	1.679×10^{-5}	N/A	12.81	1.656×10^{-5}	N/A
MEE-RTS	10^{-1}	9.52	2.322×10^{-4}	1.0249	8.99	2.302×10^{-4}	1.0225	10.93	2.337×10^{-4}	1.0101
MEE-RTS	10^{-2}	9.51	2.562×10^{-4}	1.2128	8.94	2.563×10^{-4}	1.1962	10.91	2.530×10^{-4}	1.1893
MEE-RTS	10^{-3}	9.49	3.155×10^{-4}	1.6599	8.93	3.130×10^{-4}	1.6423	10.89	3.104×10^{-4}	1.6098
MEE-RTS	10^{-4}	9.48	3.419×10^{-4}	1.9380	8.91	3.349×10^{-4}	1.9413	10.88	3.324×10^{-4}	1.8310
MEE-RTS	10^{-5}	9.47	3.849×10^{-4}	2.3892	8.90	3.530×10^{-4}	2.4786	10.87	3.687×10^{-4}	2.2041
MEE-RTS	10^{-6}	9.46	4.453×10^{-4}	2.9323	8.89	4.543×10^{-4}	3.0513	10.87	4.155×10^{-4}	2.6500
MEE-RTS	10^{-7}	9.45	4.931×10^{-4}	3.4424	8.88	5.177×10^{-4}	3.6535	10.86	7.701×10^{-4}	3.1446
MEE-RTS	10^{-8}	9.45	5.468×10^{-4}	3.9648	8.88	5.740×10^{-4}	4.2352	10.86	5.076×10^{-4}	3.4870

systems. However, retaining only the first-order Taylor expansion term inevitably introduces errors due to linearization. To extend the application, there is a need to develop an RTS-type smoother based on the MEE criterion with higher accuracy for estimating the state of nonlinear systems, which is our future work.

VII. ACKNOWLEDGMENTS

This work was funded by the NNSFC with Nos. 51975107 and 62103083, Sichuan Science and Technology Major Project No.2019ZDZX0020, and Sichuan Science and Technology Program, No. 2022YFG0343. The first two authors contributed equally to this study.

APPENDIX

The covariance of the errors $\xi_{s;t}$ and $\xi_{f;t}$ is defined as

$$\begin{cases} E[\xi_{s;t}\xi_{s;t}^T] = Cov(\xi_{s;t}) = P_{t|T}, \\ E[\xi_{f;t}\xi_{f;t}^T] = Cov(\xi_{f;t}) = P_{t|t}. \end{cases} \quad (104)$$

Combining $\xi_{s;t} = x_t - \tilde{x}_{t|T}$ and $\xi_{f;t} = x_t - \tilde{x}_{t|t}$, (52) can be rewritten as

$$\xi_{f;t} + K_t^b \tilde{x}_{t+1|t} = \xi_{s;t} + K_t^b \tilde{x}_{t+1|T}. \quad (105)$$

Taking covariance on both sides of (105), one can obtain

$$\begin{aligned} E \left[\begin{array}{c} \xi_{f;t}\xi_{f;t}^T + \xi_{f;t}\tilde{x}_{t+1|t}^T (K_t^b)^T + \\ K_t^b \tilde{x}_{t+1|t} \xi_{f;t}^T + K_t^b \tilde{x}_{t+1|t} \tilde{x}_{t+1|t}^T (K_t^b)^T \end{array} \right] = \\ E \left[\begin{array}{c} \xi_{s;t}\xi_{s;t}^T + \xi_{s;t}\tilde{x}_{t+1|T}^T (K_t^b)^T + \\ K_t^b \tilde{x}_{t+1|T} \xi_{s;t}^T + K_t^b \tilde{x}_{t+1|T} \tilde{x}_{t+1|T}^T (K_t^b)^T \end{array} \right]. \end{aligned} \quad (106)$$

Since $E[\xi_{f;t}\tilde{x}_{t+1|t}^T] = 0$ and $E[\xi_{s;t}\tilde{x}_{t+1|T}^T] = 0$ proposed in [7], (106) can be simplified to

$$\begin{aligned} E[\xi_{f;t}\xi_{f;t}^T] + K_t^b F E[\tilde{x}_{t|t}\tilde{x}_{t|t}^T] F^T (K_t^b)^T \\ = E[\xi_{s;t}\xi_{s;t}^T] + E[K_t^b \tilde{x}_{t+1|T} \tilde{x}_{t+1|T}^T (K_t^b)^T]. \end{aligned} \quad (107)$$

Substituting the fact $Cov(\tilde{x}_{t|t}) = Cov(x_t) - P_{t|t}$ and $Cov(\tilde{x}_{t+1|T}) = Cov(x_{t+1}) - P_{t+1|T}$ into (107), and we can obtain (54).

REFERENCES

- [1] S. A. Memon, W.-G. Kim, M.-S. Park, and M. Attique, "Rauch-Tung-Striebel smoothing linear multi-target tracking in clutter," *IEEE Access*, vol. 10, pp. 3007–3016, 2022.
- [2] Y. Liu, H. Wang, and W. Zhang, "Robust parameter estimation with outlier-contaminated correlated measurements and applications to aerodynamic coefficient identification," *Aerospace Science and Technology*, vol. 118, p. 106995, 2021.
- [3] K.-W. Chiang, Y.-W. Huang, C.-Y. Li, and H.-W. Chang, "An ANN embedded RTS smoother for an INS/GPS integrated positioning and orientation system," *Applied Soft Computing*, vol. 11, no. 2, pp. 2633–2644, 2011, the Impact of Soft Computing for the Progress of Artificial Intelligence.
- [4] A. Vicente, S. Zhao, and B. Huang, "Forward-backward smoothers with finite impulse response structure," *IEEE Transactions on Systems, Man, and Cybernetics: Systems*, vol. 51, no. 2, pp. 765–774, 2021.
- [5] M. P. Balenzuela, A. G. Wills, C. Renton, and B. Ninness, "A new smoothing algorithm for jump markov linear systems," *Automatica*, vol. 140, p. 110218, 2022.
- [6] H. Wang, H. Yu, M. Hoy, J. Dauwels, and H. Wang, "Variational bayesian dynamic compressive sensing," in *2016 IEEE International Symposium on Information Theory (ISIT)*. IEEE, 2016, pp. 1421–1425.
- [7] H. E. Rauch, F. Tung, and C. T. Striebel, "Maximum likelihood estimates of linear dynamic systems," *AIAA journal*, vol. 3, no. 8, pp. 1445–1450, 1965.
- [8] S. Särkkä, *Bayesian filtering and smoothing*, ser. 1. Cambridge university press, 2013, no. 3.
- [9] S. Särkkä, "Unscented Rauch-Tung-Striebel smoother," *IEEE Transactions on Automatic Control*, vol. 53, no. 3, pp. 845–849, 2008.
- [10] I. Arasaratnam and S. Haykin, "Cubature Kalman smoothers," *Automatica*, vol. 47, no. 10, pp. 2245–2250, 2011.
- [11] B. M. Bell, "The iterated Kalman smoother as a Gauss-Newton method," *SIAM Journal on Optimization*, vol. 4, no. 3, pp. 626–636, 1994.
- [12] H. Wang, H. Li, W. Zhang, J. Zuo, and H. Wang, "Maximum correntropy derivative-free robust Kalman filter and smoother," *IEEE Access*, vol. 6, pp. 70 794–70 807, 2018.
- [13] H. Wang, Y. Liu, W. Zhang, and J. Zuo, "Outlier-robust Kalman filter in the presence of correlated measurements," *Signal Processing*, vol. 193, p. 108394, 2022.
- [14] H. Wang, W. Zhang, J. Zuo, and H. Wang, "Outlier-robust Kalman filters with mixture correntropy," *Journal of the Franklin Institute*, vol. 357, no. 8, pp. 5058–5072, 2020.
- [15] A. Aravkin, J. V. Burke, L. Ljung, A. Lozano, and G. Pillonetto, "Generalized kalman smoothing: Modeling and algorithms," *Automatica*, vol. 86, pp. 63–86, 2017.
- [16] H. Wang, H. Li, W. Zhang, J. Zuo, and H. Wang, "Derivative-free Huber-Kalman smoothing based on alternating minimization," *Signal Processing*, vol. 163, pp. 115–122, 2019.
- [17] C. D. Karlgaard, "Nonlinear regression Huber-Kalman filtering and fixed-interval smoothing," *Journal of guidance, control, and dynamics*, vol. 38, no. 2, pp. 322–330, 2015.
- [18] A. Y. Aravkin, B. M. Bell, J. V. Burke, and G. Pillonetto, "An ℓ_1 -Laplace robust Kalman smoother," *IEEE Transactions on Automatic Control*, vol. 56, no. 12, pp. 2898–2911, 2011.

- [19] Y. Huang, Y. Zhang, N. Li, and J. Chambers, "A robust Gaussian approximate fixed-interval smoother for nonlinear systems with heavy-tailed process and measurement noises," *IEEE Signal Processing Letters*, vol. 23, no. 4, pp. 468–472, 2016.
- [20] —, "Robust student's t based nonlinear filter and smoother," *IEEE Transactions on Aerospace and Electronic Systems*, vol. 52, no. 5, pp. 2586–2596, 2016.
- [21] F. Zhu, C. Xue, Y. Huang, and Y. Zhang, "Robust student's t-based Rauch-Tung-Striebel smoother for non-stationary heavy-tailed measurement noises," in *2021 40th Chinese Control Conference (CCC)*, 2021, pp. 3071–3076.
- [22] Y. Huang, Y. Zhang, Y. Zhao, L. Mihaylova, and J. A. Chambers, "Robust Rauch-Tung-Striebel smoothing framework for heavy-tailed and/or skew noises," *IEEE Transactions on Aerospace and Electronic Systems*, vol. 56, no. 1, pp. 415–441, 2020.
- [23] J.-S. Hu and C.-H. Yang, "Second-order extended H_∞ filter for nonlinear discrete-time systems using quadratic error matrix approximation," *IEEE Transactions on Signal Processing*, vol. 59, no. 7, pp. 3110–3119, 2011.
- [24] W. Liu, P. P. Pokharel, and J. C. Principe, "Correntropy: Properties and applications in non-Gaussian signal processing," *IEEE Transactions on Signal Processing*, vol. 55, no. 11, pp. 5286–5298, 2007.
- [25] H. Tang and H. Li, "Information theoretic learning: Reny's entropy and kernel perspectives (Principe, j.; 2010) [book review]," *IEEE Computational Intelligence Magazine*, vol. 6, no. 3, pp. 60–62, 2011.
- [26] G. Wang, Y. Zhang, and X. Wang, "Maximum correntropy Rauch-Tung-Striebel smoother for nonlinear and non-Gaussian systems," *IEEE Transactions on Automatic Control*, vol. 66, no. 3, pp. 1270–1277, 2020.
- [27] C. Lu, W. Feng, Y. Zhang, and Z. Li, "Maximum mixture correntropy based outlier-robust nonlinear filter and smoother," *Signal Processing*, vol. 188, p. 108215, 2021.
- [28] X. Liu, Z. Ren, H. Lyu, Z. Jiang, P. Ren, and B. Chen, "Linear and nonlinear regression-based maximum correntropy extended kalman filtering," *IEEE Transactions on Systems, Man, and Cybernetics: Systems*, vol. 51, no. 5, pp. 3093–3102, 2021.
- [29] W. Wang, C. K. Tse, and S. Wang, "Generalized correntropy sparse gauss-hermite quadrature filter for epidemic tracking on complex networks," *IEEE Transactions on Systems, Man, and Cybernetics: Systems*, vol. 52, no. 5, pp. 2770–2778, 2022.
- [30] D. Erdogmus and J. C. Principe, "An error-entropy minimization algorithm for supervised training of nonlinear adaptive systems," *IEEE Transactions on Signal Processing*, vol. 50, no. 7, pp. 1780–1786, 2002.
- [31] J. He, G. Wang, K. Cao, H. Diao, G. Wang, and B. Peng, "Generalized minimum error entropy for robust learning," *Pattern Recognition*, vol. 135, p. 109188, 2023.
- [32] G. Wang, X. Yang, L. Wu, Z. Fu, X. Ma, Y. He, and B. Peng, "A kernel recursive minimum error entropy adaptive filter," *Signal Processing*, vol. 193, p. 108410, 2022.
- [33] J. He, G. Wang, B. Peng, Q. Sun, Z. Feng, and K. Zhang, "Mixture quantized error entropy for recursive least squares adaptive filtering," *Journal of the Franklin Institute*, vol. 359, no. 3, pp. 1362–1381, 2022.
- [34] G. Wang, B. Peng, Z. Feng, X. Yang, J. Deng, and N. Wang, "Adaptive filtering based on recursive minimum error entropy criterion," *Signal Processing*, vol. 179, p. 107836, 2021.
- [35] J. He, G. Wang, H. Yu, J. Liu, and B. Peng, "Generalized minimum error entropy kalman filter for non-gaussian noise," *ISA Transactions*, 2022.
- [36] L. Dang, B. Chen, Y. Xia, J. Lan, and M. Liu, "Dual extended kalman filter under minimum error entropy with fiducial points," *IEEE Transactions on Systems, Man, and Cybernetics: Systems*, vol. 52, no. 12, pp. 7588–7599, 2022.
- [37] B. Chen, X. Liu, H. Zhao, and J. C. Principe, "Maximum correntropy Kalman filter," *Automatica*, vol. 76, pp. 70–77, 2017.
- [38] Z. Feng, G. Wang, B. Peng, J. He, and K. Zhang, "Novel robust minimum error entropy wasserstein distribution Kalman filter under model uncertainty and non-gaussian noise," *Signal Processing*, p. 108806, 2022.
- [39] L. M. Silva, C. S. Felgueiras, L. A. Alexandre, and J. M. de Sá, "Error entropy in classification problems: A univariate data analysis," *Neural computation*, vol. 18, no. 9, pp. 2036–2061, 2006.
- [40] I. Santamaría, D. Erdogmus, and J. C. Principe, "Entropy minimization for supervised digital communications channel equalization," *IEEE Transactions on Signal Processing*, vol. 50, no. 5, pp. 1184–1192, 2002.
- [41] L. Dang, B. Chen, S. Wang, W. Ma, and P. Ren, "Robust power system state estimation with minimum error entropy unscented Kalman filter," *IEEE Transactions on Instrumentation and Measurement*, vol. 69, no. 11, pp. 8797–8808, 2020.
- [42] L. Dang, B. Chen, Y. Huang, Y. Zhang, and H. Zhao, "Cubature Kalman filter under minimum error entropy with fiducial points for INS/GPS integration," *IEEE/CAA Journal of Automatica Sinica*, vol. 9, no. 3, pp. 450–465, 2021.
- [43] B. Chen, L. Dang, Y. Gu, N. Zheng, and J. C. Principe, "Minimum error entropy Kalman filter," *IEEE Transactions on Systems, Man, and Cybernetics: Systems*, vol. 51, no. 9, pp. 5819–5829, 2019.
- [44] G. Wang, B. Chen, X. Yang, B. Peng, and Z. Feng, "Numerically stable minimum error entropy Kalman filter," *Signal Processing*, vol. 181, p. 107914, 2021.
- [45] G. Wang, N. Li, and Y. Zhang, "Maximum correntropy unscented Kalman and information filters for non-Gaussian measurement noise," *Journal of the Franklin Institute*, vol. 354, no. 18, pp. 8659–8677, 2017.
- [46] T. S. Alexander, *Adaptive signal processing: theory and applications*. Springer Science & Business Media, 2012.
- [47] J. He, G. Wang, X. Zhang, H. Wang, and B. Peng, "Maximum total generalized correntropy adaptive filtering for parameter estimation," *Signal Processing*, vol. 203, p. 108787, 2023.
- [48] S. Peng, B. Chen, L. Sun, W. Ser, and Z. Lin, "Constrained maximum correntropy adaptive filtering," *Signal Processing*, vol. 140, pp. 116–126, 2017.
- [49] X. Fan, G. Wang, J. Han, and Y. Wang, "A background-impulse kalman filter with non-gaussian measurement noises," *IEEE Transactions on Systems, Man, and Cybernetics: Systems*, pp. 1–10, 2022.
- [50] Udacity, "Udacity's self-driving car simulator," <https://github.com/udacity/self-driving-car-sim>, 2017.